Design and Fabrication of an Optical Pressure Micro Sensor for Skin Mechanics Studies

By

Siddarth Kumar

B.Tech. Production and Industrial Engineering (2004)
Indian Institute of Technology, Delhi INDIA

Submitted to the Department of Mechanical Engineering
in Partial Fulfillment of the Requirement for the Degree of
Master of Science in Mechanical Engineering

at the

Massachusetts Institute of Technology

June 2006

Signature of Author_____
Department of Mechanical Engineering
May 24, 2006

Certified by_____
Dr. Mandayam A. Srinivasan
Senior Research Scientist, Department of Mechanical Engineering
Thesis Supervisor

Accepted by_____
Professor Lallit Anand
Chairman, Department Committee on Graduate Students

Design and Fabrication of a PDMS based Optical Pressure Micro sensor for Skin Mechanics Studies.

by

Siddarth Kumar

Submitted to the Department of Mechanical Engineering
on May 24, 2006 in Partial Fulfillment of the Requirements for the
Degree of Master of Science in Mechanical Engineering

Abstract

The mechanics of skin is as central to touch as optics is to vision and acoustics is to hearing. With the advent of novel imaging technologies such as the Optical Coherence Tomography (OCT), we are now able to view structures within the skin to a resolution of a few microns in vivo and non-invasively. To fully understand the role of biomechanics of the skin in interpreting touch, we need to develop a quantitative understanding of how spatio temporal loads imposed on the surface of the skin are transmitted to mechanoreceptor locations within the skin. The following thesis presents a description of the design and fabrication of an Optical Pressure Sensor Device to be used in conjunction with an Optical Coherence Tomography Apparatus to quantify loads incident on the fingerpad surface.

The Optical Pressure Sensor is a five layer PDMS based device having a total thickness of 150 microns. It consists of two layers of a textured pattern separated by a layer of "Soft" PDMS of thickness 100 microns. The top and bottom protective layers are of PDMS and have a thickness of 20 microns each. "Soft" PDMS is a combination of PDMS and the silicone oil "Fluid 200" and has a Young's Modulus less than that of Human Skin. The entire device is fabricated bottom up on a silicon wafer using soft lithography techniques and the textured pattern is imprinted onto the PDMS using photolithography techniques.

This flexible pressure sensor is designed to be used on the fingerpad skin to determine the pressure distribution due to incident loads. The sensor is placed between the OCT head and the finger pad to be imaged. The OCT head (along with the indenter) acts as the mechanical stimulus and is used to indent the finger pad. As a result of this stimulus, the human skin along with the pressure sensor gets deformed and both these deformations are picked up by the OCT image. The deflection between the two bands of patterns is used to estimate the stress at the pressure sensor and skin interface through the development of a continuum mechanics model which is also developed and introduced in this thesis. The manufactured device is tested and calibrated for use with the fingerpad.

Thesis Supervisor: Dr. Mandayam A Srinivasan
Title: Senior Research Scientist, Department of Mechanical Engineering, MIT

Acknowledgements

The past couple of years as a graduate student in the department of Mechanical Engineering at MIT have been a wonderful experience for me mostly due to the wonderful people I have come across. I have learnt a lot and have made some real good friends along the way.

First and foremost, I would like to thank my advisor, Dr. Srinivasan, for his support over the past two years. He has been instrumental in shaping my research through his guidance and has given me confidence to explore new ideas without the fear of failure while always keeping me aware of the big picture. I really appreciate the freedom he has given me in the lab. I have grown academically and have learnt a lot. I shall carry these lessons with me for years to come.

This project involved significant experimental work (micro-fabrication) none of which would have been possible without the guidance of Dr. Gang Liu who introduced me to the wonderful world of micro fabrication and soft lithography. I am thankful for his help every step of the way: - right from the device design and fabrication till its testing and calibration. I really enjoyed all the discussions we had about research and life in general.

I would like to thank Kurt Broderick for teaching me and showing me the ropes at EML. I appreciate his wonderful suggestions in my times of difficulty.

I cannot thank enough Leslie Regan, Joan Kravit and the entire Grad Office for being there and for providing all the help and support right from the time I was unfunded and new on campus. They helped make MIT feel like a home away from home.

None of this would have been possible to survive without the friends I made along the way. I have forged lifelong friendships with Piyush, Sunil, Ilkay (the coolest guy I have ever met) and Mayank. I will always remember all the experiences we shared together. I have made a lot of friends and sadly cannot name them all but will have to mention Abhinandan, a real cool guy and my best tennis partner (we were unbeatable); and of course, Hemanth, for his unusual humor (which rubs some people the wrong way).

Last and definitely not the least, I would like to thank my parents: my mother, Dr. Vanaja Kumar, and father, Prof. TM Vinod Kumar, for having complete faith in me even in times of great uncertainty. Their unflinching support over the past 23 years has been humbling and I am grateful for all they have done for me. I would like to thank my elder brother, Jaisurya and twin, Dr. Srikant (fresh out of med school) for keeping me grounded in times of success and helping me rise in times of failure.

Contents

List of Figures

Chapter 1

Introduction

This thesis presents the design, fabrication and testing of a novel PDMS based pressure micro-sensor capable of estimating the stress distribution due to an unknown load over an area of few microns. The pressure sensor is to be used to estimate the stress distribution due to a micro indenter on the skin.

1.1 Motivation

The sequence of events that lead to tactile sensing is as follows: when the skin comes into physical contact with an object, the epidermis and dermis undergo deformations (they are subject to a strain field). This deformation of the matrix leads to the distortion of the embedded mechanoreceptors.

These distortions trigger specific responses from the mechanoreceptors which transmits the sensory information to the central nervous system (CNS) via afferents nerve fibers in the arm. Tactile perception takes place when the brain decodes this sensory information.

In order to gain a fundamental understanding of the origins and mechanisms of the human tactile sense, one needs to study the role of each of the components involved in the tactile system. A quantitative understanding of how spatio temporal loads, imposed on the surface of the skin, are transmitted to mechanoreceptor locations within the skin needs to be developed in order to fully understand the role of biomechanics of the skin in touch. One way to completely study the tactile system is to observe how the mechanoreceptor behaves in response to various external stimuli on the skin.

With new imaging technologies such as Optical Coherence Tomography (OCT), we are now able to view structures within the skin to a resolution of a few microns. This gives us an opportunity to observe and study deformations near mechanoreceptor locations when the skin surface is subject to different defined loads in vivo and non-invasively.

However, one needs to develop a method of quantifying the load subjected on the finger pad skin in the same order as the field of view of the OCT which is 1000 μm x 1000 μm to micron resolution.

The focus of this thesis is to develop a device that will help us to quantify the input spatial pressure distribution that a stimulus exerts on the fingerpad, enabling us to accurately quantify the input stress subjected on the fingerpad surface.

1.2 Brief Review of the Human Tactile system

Touch in the human skin is interpreted through peripheral nerve endings embedded in the skin. The human fingertip is highly innervated with these sensory receptors which map to large areas in the cortex. There are four major types of such organelles, termed as mechanoreceptors in the skin. Each of the four mechanoreceptors innervating the hand is sensitive to a distinctly different tactile perceptual function.

Thus, each of these mechanoreceptors conveys certain aspects of touch such as pressure, vibration, tension to the central nervous system. Tactile perception can be understood as a sum of these functions.

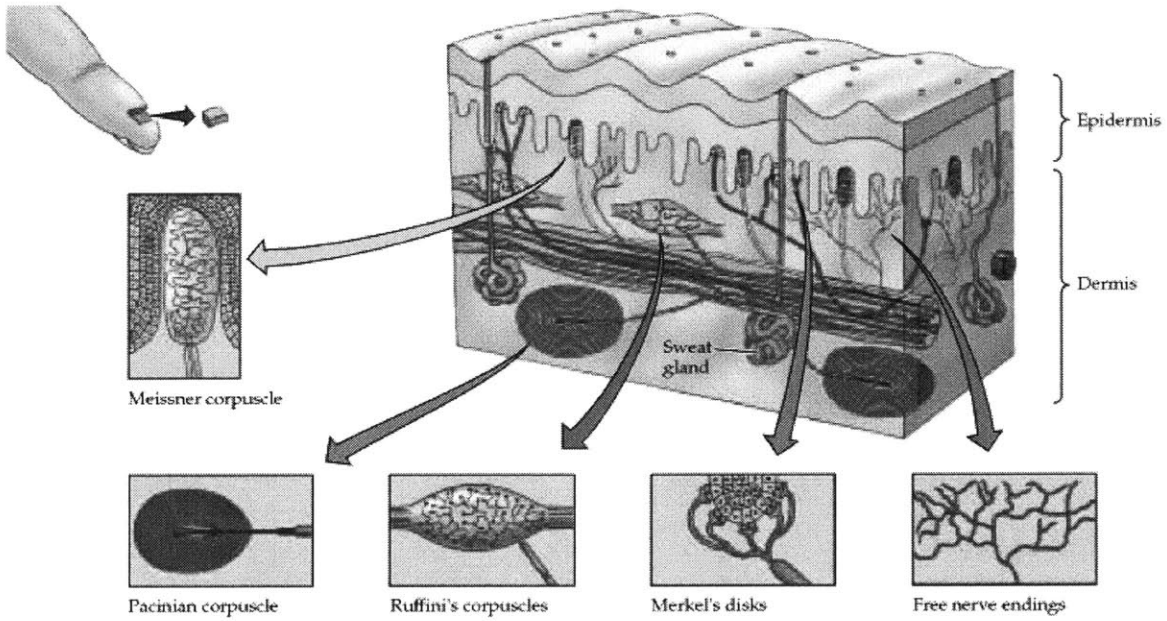

Figure 1.1: The major types of Mechanoreceptors embedded in the skin (From Neuroscience 2003)

As shown in the above figure, there are four mechanoreceptors that innervate the skin: Merkel Disks, Meissner Corpuscles, Ruffini corpuscles and Pacinian Corpuscles. Apart from these there are also free nerve endings and nocireceptors that are sensitive to pain.

These receptors are referred to collectively as low-threshold (or high-sensitivity) mechanoreceptors because even weak mechanical stimulation of the skin induces them to produce action potentials. All low-threshold mechanoreceptors are innervated by relatively large myelinated axons, ensuring the rapid central transmission of tactile information.

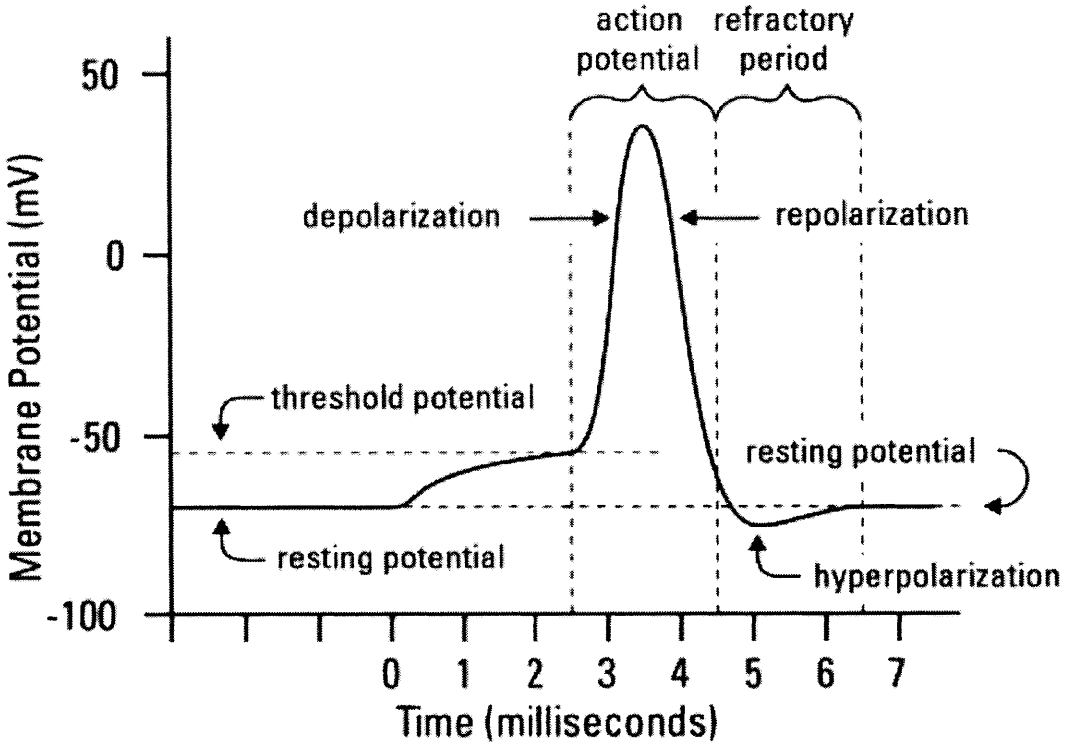

Figure 1.2: A Typical Action Potential in a Neuron when stimulated (From Neuroscience 2003)

Nerve cells communicate information to the brain via a series of electrical discharges called action potentials. Mechanoreceptors are characterized based in their behavior in response to constant stimuli (step input). Those receptors that exhibit a very slowly rate of decay in their discharge rate are termed as slowly adapting (SA) and those that have a fast rate of decay are termed as Rapidly adapting (RA).

Merkel Disks innervate the skin quite densely (about 100 per cm^2 in human and monkey fingertip[7]) They are a type of SA-I afferents and respond to sustained indentation whose discharge rate is linearly related to the depth of indentation. They are sensitive to points, edges and curvatures. Their receptive field diameter is around 2-3 mm and can resolve spatial details of the order of .5 mm. Meissner Corpuscles are responsible for form and texture perception.

The Pacinian corpuscle comprises of a large onion like structure which encapsulates a single nerve ending that is sensitive to deformation on the nanometer scale. Pacinian corpuscles are involved in the discrimination of fine surface textures or other moving stimuli that produce high-frequency vibration of the skin. The most sensitive pacinian afferents respond to 10nm of skin motion or less at 200 Hz [10]. They are two orders of magnitude sensitive to RA afferents.

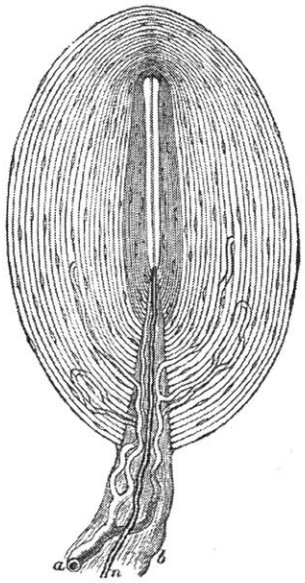

Figure 1.3: Pacinian corpuscle (From Gray's anatomy of the human body (30th edition))

The layers function as a series of high pass mechanical filters protecting the nerve ending from large magnitude strains exerted by daily activities [4]. They are distributed throughout the palm and finger (about 350 per finger and about 800 in the palm [7]). Because of their deep locations and high sensitivity their spatial resolution is difficult to define and their receptor field is the entire hand. They are even sensitive to distant events through transmitted vibrations [7]. If you hold a stick and scrape it slowly at a rough surface, you feel the vibrations at the tip of the stick, it is the pacinian corpuscles that are responding to this distant stimuli.

The Meissner corpuscles are the receptors closest to the surface of the skin and are located close to the ridge separating the dermis from the epidermis. They innervate the skin more densely than the Merkel disks (about 150 per cm^2 in human and monkey

fingertip[7]). They are Rapidly Adapting and unlike Merkel cells are insensitive to static skin deformation.

They are four times more sensitive to dynamic deformation than SA1 type afferents. They have a receptor field of about 3-5mm in diameter and respond to stimuli uniformly over their entire receptor field. They have poor spatial resolution. They are known to detect and discriminate low frequency vibrations [7]. They detect slip between the skin and an object held in the hand [8] and provide feedback to the CNS for grip control[9].
The Ruffini corpuscle is present in the dermis and has a spindle like structure tied to the collagen matrix making it sensitive to skin stretch. It functions similar to golgi tendons providing stretch information to the CNS.

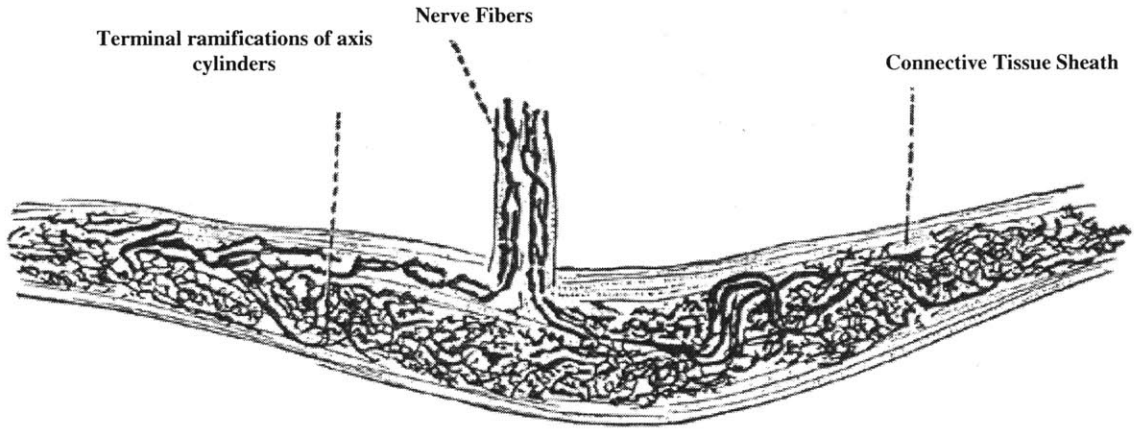

Figure 1.4: Nerve ending of Ruffini (From Gray's anatomy of the human body (30th edition))

There seems to be a division of function among the four cutaneous afferent systems that innervate the hand [7]. Information regarding the spatial structures of objects and surfaces essential for form and texture perception is sent to the brian via SA-1 type afferents. Rapidly adapting (RA) mechanoreceptors provide information regarding motion signals from the whole hand whereas pacinian corpuscles provides information regarding vibrations transmitted to the hand from objects contacting the hand or those grasped by the hand.

1.3 Current Research

As has been mentioned in the previous section, tactile information, as is perceived by us, is a result of the combination of the signals sent to the CNS through each type of tactile mechanoreceptor. This division of function also seems to suggest that different aspects if touch maybe processed at distinct locations of the brain though this has yet to be validated.

A major challenge is to map and understand the central pathways processing the information provided by the four primary afferent systems. One needs to find a way to selectively stimulate each of the afferent systems with meaningful stimuli in order to decipher the pathways the receptors use to send signals to the brain. This is complicated by the fact that the receptors are difficult to identify within the skin. Although they number in the thousands they are deeply innervated in the skin and are difficult to locate. Imaging technology such as Optical Coherence Tomography now enables us to look a depth of around 1000 μm within the skin to a axial resolution of 3 microns and a lateral resolution of 5 microns. Even with such technology it is difficult to identify these receptors.

Early studies attempting to relate mechanical displacements to resultant mechanoreceptor impulse patterns were conducted by Fuller et al [14] in 1966. He studied the response of mechanoreceptors to mechanical displacements applied to a cat's pad. Goodwin et al [15] studied the population response of Rapidly Adapting afferents in the glabrous skin of a monkey. However, Neural activity in response even to simple stimuli is found to be quite complex. The reason for this is the complex structure of the skin.

Even simple loads applied at the surface of the skin would produce complex stress fields within the skin matrix and hence trigger one or more of the tactile receptors. It is thus essential to understand skin mechanics before trying to reconstruct population responses in response to tactile stimuli.

Detailed studies attempting to characterize the spatial tactile resolution of touch receptors, taking into account skin mechanics, were performed by Phillips and Johnson [11, 12 and 13]. A continuum mechanic model of the skin was developed to predict the subcutaneous stresses and strains produced by bars, edges and gratings. The discharge rates of the mechanoreceptors were assumed to be proportional to the magnitude of the strain at proposed mechanoreceptor locations and this discharge rate was compared to experimental values.

The structure of the fingertip is quite complex. It consists of two layers of skin: the dermis and epidermis consisting of subcutaneous tissues including randomly oriented collagen fibers, sweat glands and fat cells. When an object is in contact with the fingerpad, the tactile information of the object is contained in the spatial temporal load distribution on the skin which results in a stress state at receptor locations within the skin.

All the above mentioned studies dealt with the responses of receptors to known stimuli. Not many experiments were performed to observe and estimate the load distribution on the skin when an object comes into contact with it and the corresponding strains within the skin matrix.

Studies regarding the role of fingertip geometry in the transmission of tactile signals were conducted by Srinivasan et al [16]. Detailed two and three dimensional Finite Element models of the primate fingertip were constructed by Dandekar et al [5, 6] addressing the issue of skin mechanics in tactile sensing.

Still experimental techniques need to be developed that address the problem of quantifying accurately the load distribution directly on the fingerpad.

1.4 Review of Pressure Sensor Technology

This section presents a review of commercially available pressure sensors, their working principles, characteristics, limitations as well as a brief review of tactile sensors recently developed by researchers around the world.

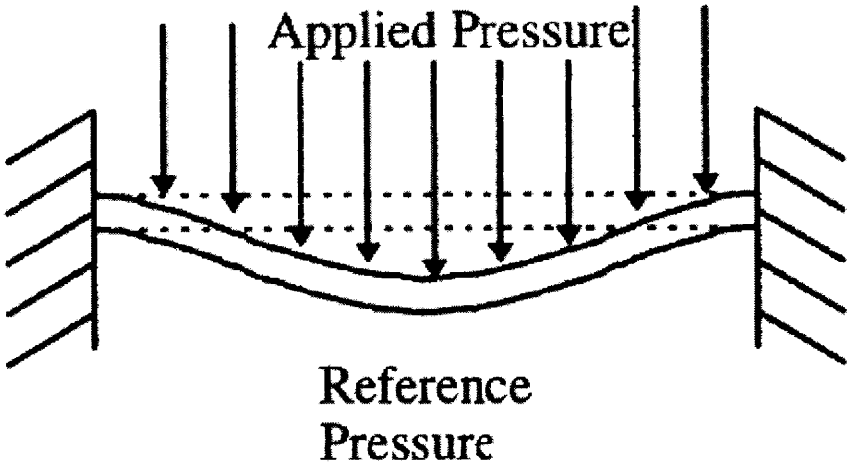

Figure 1.5: A functional schematic of a typical pressure sensor diaphragm

In recent times, with the advent of MEMS technology, miniaturized silicon based pressure sensors are popular and are widely produced. MEMS based pressure sensors currently dominate the market for greater than atmospheric pressure sensors.

In early macroscopic sensors, pressure information was converted to the motion of a mechanical element which was recorded and calibrated to the incident pressure. These sensors were based on diaphragms where the deflection of the diaphragm gave information regarding the incident pressures.

Strain gauges were commonly used on diaphragm based devices to pick up the deflection of the diaphragm. In capacitive sensors, the diaphragm acted as a pair of capacitive plates and a change in the deflection of the diaphragm translated into a change in capacitance which was picked up and calibrated to the incident pressure value.

Other sensors such as Bourdon tubes (shown in figure 2.2 (f) and (g)) and straight walled tubes deflected or expanded in the presence of increased pressure.

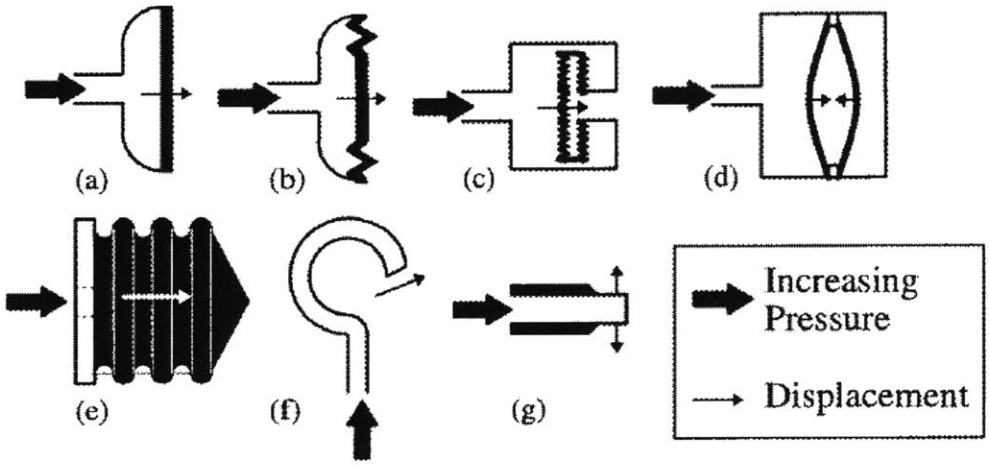

Figure 1.6: Various macroscopic pressure sensors (from [16]) (a) simple diaphragm; (b) corrugated diaphragm sensor; (c) capsule sensor; (d) capacitive sensor; (e) bellows; (f) Bourdon tube; (g) Straight tube.

Many of the MEMS based micro-machined pressure sensors are miniaturized versions of the macroscopic sensors mentioned above (and also primarily diaphragm based). Most of these micro-sensors are manufactured on silicon substrates. This is due to the excellent mechanical properties of single crystal silicon such as high strength, high stiffness, high mechanical repeatability and no mechanical hysteresis. In addition to this, the easy availability of silicon also made it an ideal substrate for manufacturing MEMS based sensors.

In 1954, C. S. Smith [18] reported piezoelectric properties of silicon and germanium where a change in resistance was observed in response to an applied stress. This lead to the development of semiconductor based pressure sensors. Metal diaphragms were slowly replaced by single crystal diaphragms with diffused piezeresistors that picks up the deflection of the diaphragm.

Capacitive sensors were based on parallel plate capacitors. A functional image of a typical pressure sensor is shown in figure 2.3 along with its capacitive- pressure curve. For small deformations, it can be seen that the capacitive pressure curve can be approximated to a linear curve. The advantage of capacitive sensors over piezoelectric sensors is increased pressure sensitivity and decreased temperature sensitivity [20].

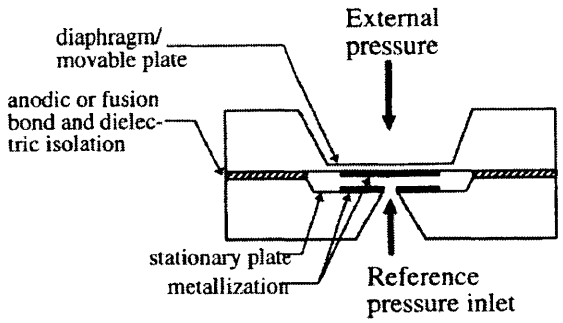

Figure 1.7: A cross section schematic of a typical capacitive pressure sensor (from [19])

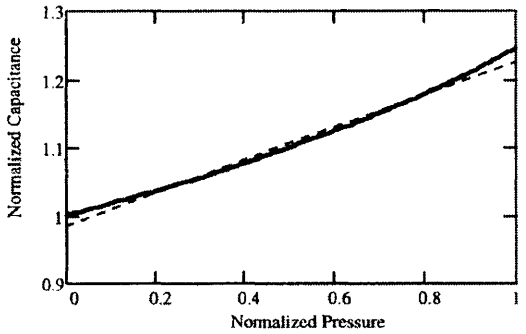

Figure 1.8: The Capacitive- pressure curve for a capacitive sensor with a circular diaphragm (from [19])

Silicon based optical pressure sensors were developed by Dzuiban et al [21] and Hoppe et al [22]. These sensors measure pressure by observing deflections by Mach-Zehnder interferometry and Fabry-Perot interferometry [23]. These sensors are very accurate however, calibrating the sensor as well as aligning the optical components of the setup is challenging and the sensors do suffer from temperature sensitivity problems.

Most of the above mentioned sensors are used to measure normal pressure of incident loads and none of them address the problem of measuring shear. Further theses sensors are planar and are not deformable.

Optical sensors have been developed in the recent past to detect slip [22]. Kyber and Chappel developed a slip sensor based on forced oscillations [23]. Dubey and Crowder developed a dynamic tactile sensor based on photo elastic effects [24]. Figure 2.5 illustrates a schematic of this sensor.

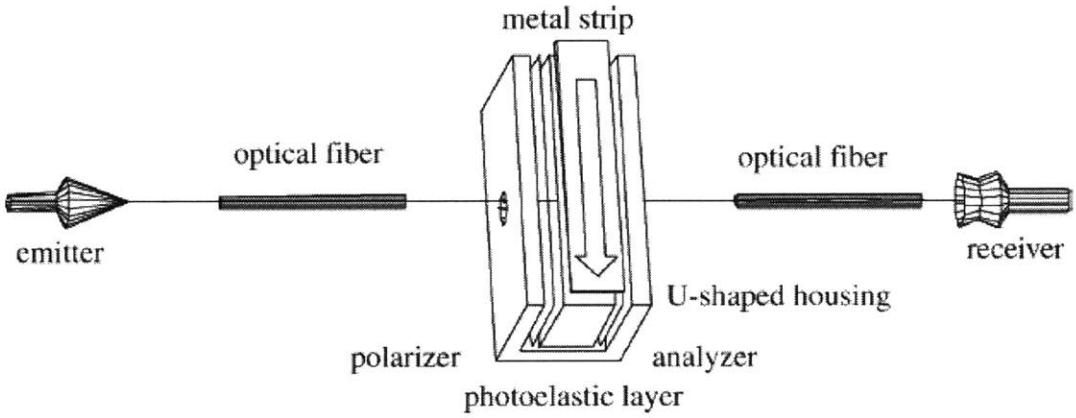

Figure 1.9: The slip sensor designed by Dubey and Crowder[24]

In the recent past, sensors also have been developed to detect shear alone. Noda et al [25] developed a shear stress sensor using a Piezoresistive cantilever embedded within an elastic polymer PDMS. Each standing cantilever follows the deformation of the elastic matrix. Piezoresistors at the hinges of the cantilever detect the deformation of the cantilever and this deformation is calibrated to the incident shear.

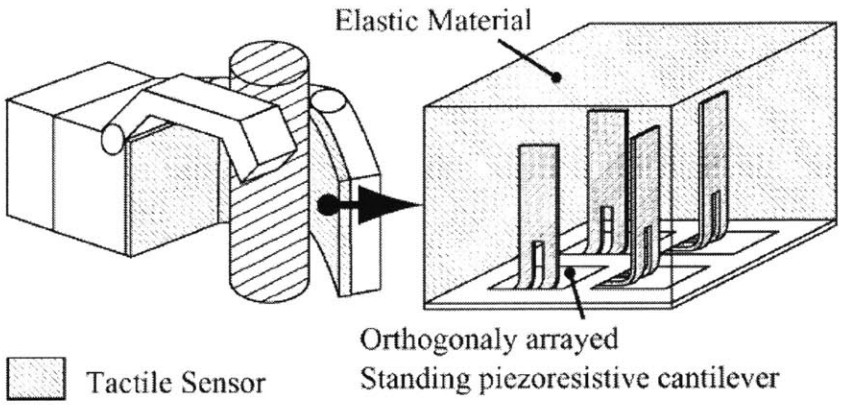

Figure 1.10: The tactile shear sensor developed by K. Noda et al [25]

A distributed pressure sensor has also been developed specifically for biomechanical applications by Pawluk et al [28] at Harvard University for biomechanical applications. It is a type of capacitive sensor consisting of 8 element by 8 element design with an elemental spacing of 2 mm.

1.5 Shortcomings of conventional sensors

A large number of pressure and force sensors have been developed with different working ranges, interfaces and operating conditions. As has been mentioned above, sensors have been developed to measure slip and shear in addition to normal pressure distributions.

However, there is a need for the development of thin and flexible sensors for biomechanical applications (such as in skin mechanics studies). These sensors are required to be used to measure the interface pressure between soft objects (skin) and indenters with high resolution over a small spatial area. Conventional sensors cannot be used for these applications owing to their rigidity, size and incompatibility.

This thesis attempts to address some of these problems through the development of a thin flexible pressure sensor capable of measuring shear and normal pressure distributions over a small spatial area of .25 mm^2 due to small loads.

1.6 Thesis Overview

This thesis deals with the design and fabrication of a PDMS based Optical Pressure Sensor and its application to study finger ridge deformation. The device is used in conjunction with an Optical Coherence Tomography setup.

Chapter 1 gives a brief description of the human tactile system followed by a brief review of the progress in the study of the tactile system and the role of skin biomechanics in receptor response.

Chapter 2 entails the design aspects of the sensor along with its working principle. It describes the working principle of the OCT apparatus followed by a discussion of the design issues of the sensor.

Chapter 3 is concerned with the development of a continuum mechanics model to predict stress at the sensor finger interface.

Chapter 4 deals with the fabrication aspects of the sensor. It gives an overview of the basic soft lithography techniques used as well as process step modifications

Chapter 5 describes the experiments performed to test and calibrate the sensor. It also describes the image processing procedures used on the OCT images to determine the displacements.

Chapter 6 summarizes the work done citing contributions along with areas of future work and a discussion of the application of the sensor to measure loads of different shapes with the finger.

Chapter 2

Sensor Design and Measurement principle

This chapter describes the design and measurement principle of the sensor. As this sensor is designed to work with an Optical Coherence Tomography (OCT) apparatus, we begin with a brief description of OCT technology.

2.1 Optical Coherence Tomography

Optical coherence tomography (OCT) is an interferometry based biomedical imaging technique used for non-invasive tissue imaging. It offers sub-micrometer axial and lateral resolution with a penetration depth of a few millimeters. In principle it is analogous to ultrasonic B mode imaging, except backscattering of light is detected rather than sound [2] utilizing interferometry techniques.

The OCT apparatus can image microscopic structures in tissues at depths beyond the reach of conventional bright field and confocal microscopes [1]. The apparatus has been used to image structures as deep as 1-2 mm in highly scattering tissues such as the skin.

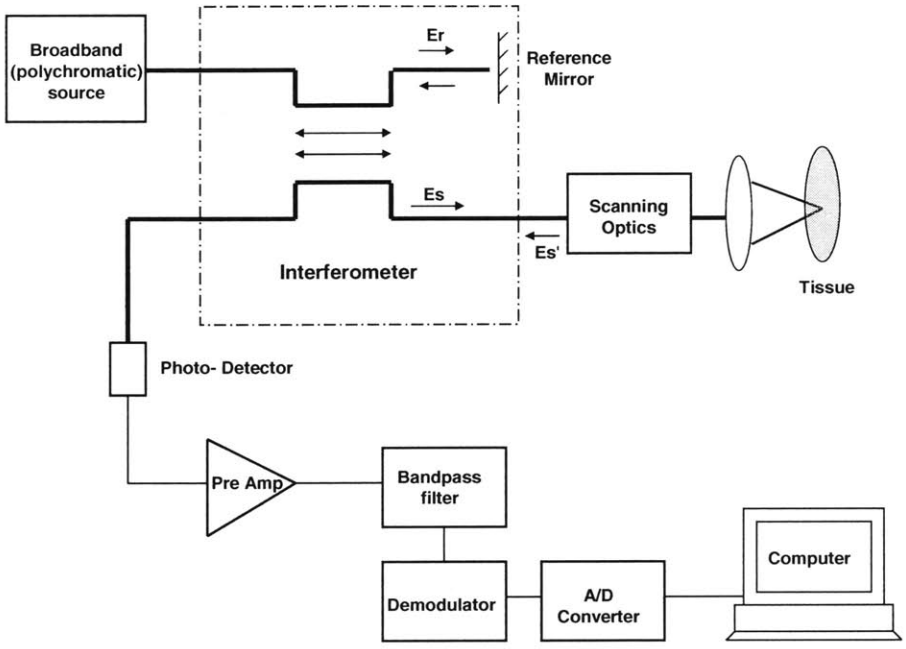

Figure 2.1: Component blocks of an OCT system (adapted from [1])

The major hardware components of the OCT system are light Source, the interferometer and the scanning optics. The light sources commonly used for OCT imaging are characterized by having emission in the near IR region of the spectrum. It is at this spectral range in which the penetration of light into the tissue is adequate. The latest generation of OCT systems employ mode locked Ti: Al_2O_3 and Cr^{4+}: forsterite lasers enabling fast imaging with high resolution. The most common interferometer configuration employed today is the fiber-optic Michelson interferometer.

The interferometer splits a broadband source field into a reference field Er and a sample Field Es. The sample field focuses through the scanning optics and objective lens to some point below the tissue surface. After scattering back from the tissue, the modified sample field Es' mixes with Er on the surface on the photo-detector [1]. This information is used to generate the image of the tissue structure.

2.2 Optical Pressure Sensor Design Issues

This section details the description of the design of the Optical Pressure Sensor Device. As has been mentioned before, we will use this in conjunction with an Optical Coherence Tomography (OCT) apparatus to determine the pressure distribution on the finger pad of a Human finger for Skin Bio Mechanics studies. Before we go into that we must first recognize the design parameters and requirements

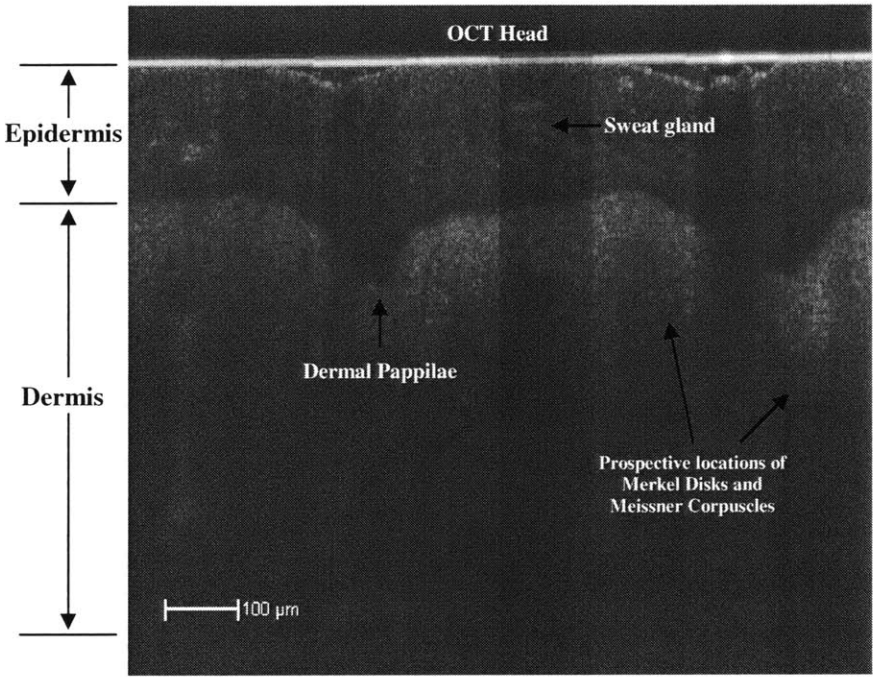

Figure 2.2: An OCT image of the human finger

Let us first look at an OCT image of the human finger. The field of view of the OCT image is 1000 microns depth by 1000 microns width. The instrument has a horizontal resolution of 5 microns and a vertical resolution of 3 microns.

The dermal papilla which separates the dermis from the epidermis is clearly visible. Other features such as sweat glands are also visible. The prospective locations of the mechanoreceptors: Merkel Disks and Meissner Corpuscles are around 300-400 microns below the surface of the skin.

The current OCT apparatus cannot image features 600 microns below the surface of the skin owing to the opaqueness of the skin. Now, the pressure sensor is to be placed between the OCT head and the finger. The stimuli would be placed between the sensor and the fingertip. A functional schematic of this setup is described in figure 2.3 for clarity.

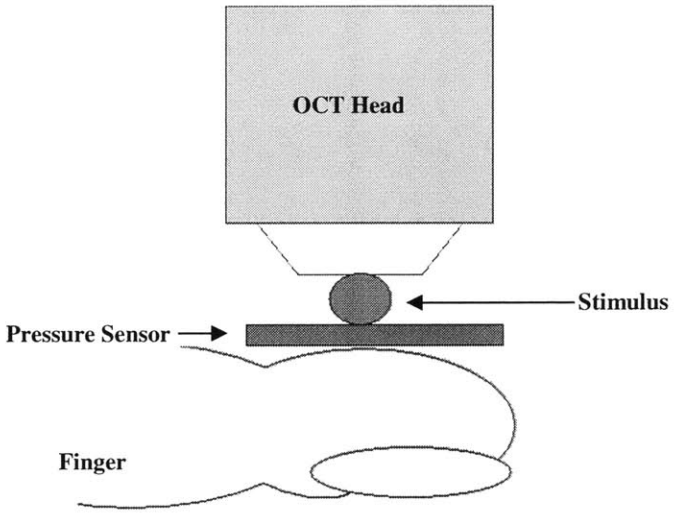

Figure 2.3: Functional Schematic of the Setup

Taking these constrains into account we arrive at the following conclusions. The OCT can image clearly about 600 microns below the surface of the skin. The total field of view of the OCT is about 1000 microns (depth).

Thus, the sensor which we design must not have a depth of greater than 400 microns. Further the sensor must be as transparent as possible so as to allow maximum penetration of light within the skin.

The OCT functioning is analogous to that of an ultrasound apparatus with sound being substituted by light. The more opaque the sensor, the more scattered the light passing through the sensor from the OCT head will be, resulting in a weaker image.

As has been mentioned above, capacitive sensors measure pressure based on the change in capacitance between two metallic layers. As the distance between the metallic layers change, so does the capacitance and hence this is converted to pressure. We use the same principle substituting change in capacitance with change in distance between certain features.

Now, the OCT image gives us an in vivo cross sectional image of the pressure sensor when we place it in front of the OCT head. We propose embedding certain features within the sensor which must have dimensions greater than the resolution of the sensor. The horizontal resolution of the sensor is 5 microns and the vertical resolution is 3 microns. Thus the features should be greater than 5 microns in width and 3 microns in height. In addition to all this as the sensor is to be used with a finger, it is required to be flexible to conform to the finger pad geometry during use. As the sensor is to be used with the skin, it is to be more deformable than the skin. Thus the effective modulus of the sensor must be less than 0.5 M Pa. We now explore the materials needed to fabricate the sensor.

2.3 Material Selection and Manipulation

Based on the above mentioned factors, we decided to manufacture a polymer based transparent pressure sensor. This would enable the sensor to be deformable and able to conform to various finger geometries. The polymer that we decided to use to manufacture the sensor was the transparent silicon based organic polymer poly di-methyl siloxane or PDMS (Sylgard(R) 184 Silicone elastomer kit from Dow Corning). It is optically clear, and is known to be inert, non-toxic and non-flammable.

A major assumption needed to simplify the modeling of the sensor is that is that within the applied strain limits, the material (PDMS) is assumed to be linearly elastic. We perform a uniaxial compression test of different samples of PDMS diluted with the silicone oil Fluid 200.

PDMS is made up of two parts, a curing agent and a polymer. PDMS samples were prepared mixing the curing agent and the polymer base in the ratio of 1:10. We also add to this, the silicone oil "fluid 200". The addition of this is done to change the Young's modulus of the polymer making it softer. This mixture was then placed in a degasser for 20 minutes to remove air bubbles.

The degassed mixture was placed in cylindrical cups of diameter ** and kept in a 65 degree oven for 2 hours to cure. Using the above procedure, samples were made mixing PDMS with fluid 200 in the ratio 30%, 40%, 50%, 60%, 70%, 80% and 90% by weight.

All these samples were subjected to a uniaxial compression test. A Z-stage was used to compress the sample between two parallel plates. A load cell was used to measure the resistive load exerted by the compressive sample.

The strains applied to the sample didn't exceed 20% which is the estimated ceiling of the working range of our pressure sensor. Figure 2.4 depicts the results of the uniaxial compression tests.

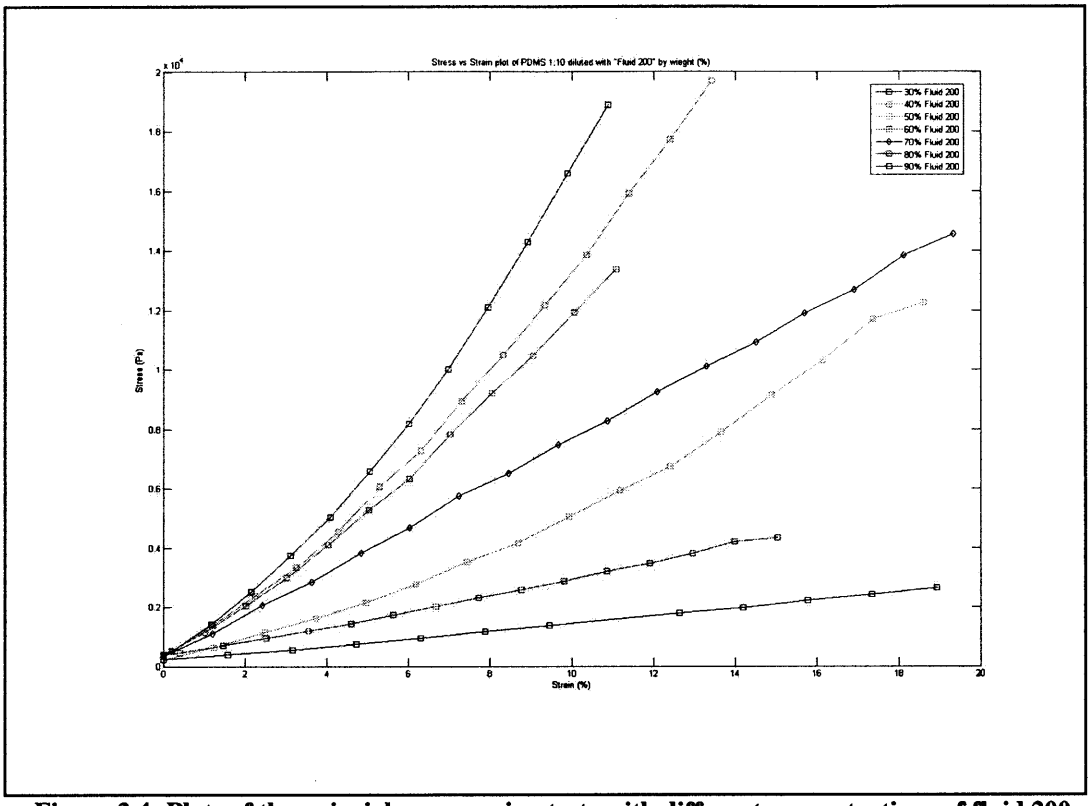

Figure 2.4: Plots of the uniaxial compression tests with different concentrations of fluid 200 with PDMS.

We observe that the behavior is fairly linear. For small displacements, we can take the assumption that PDMS can be approximated as a linear elastic material. We will this assumption to derive a continuum mechanics based model of the designed sensor in section 2.5.

PDMS diluted with 70 % fluid 200 was used to fabricate the sensor. Another sensor was fabricated with pure PDMS (1:10).

2.4 Design of the sensor

The design of the sensor is described below. The Optical Pressure Sensor is a five layer device having a total thickness of about 150 microns. A schematic of its structure is described in Figure 2.3. The sensor primarily consists of the transparent polymer PDMS.

It consists of two layers of patterned photoresist (which would act as the features) separated by a layer of Soft PDMS of thickness 100 microns. Soft PDMS is a combination of PDMS and the Silicone oil "Fluid 200" (70% by weight) and has a Young's Modulus less than that of Human Skin (~0.5MPa). The modulus of the soft polymer was found to be 0.075 M Pa.The top and bottom protective layers are of PDMS and have a thickness of 25 microns each.

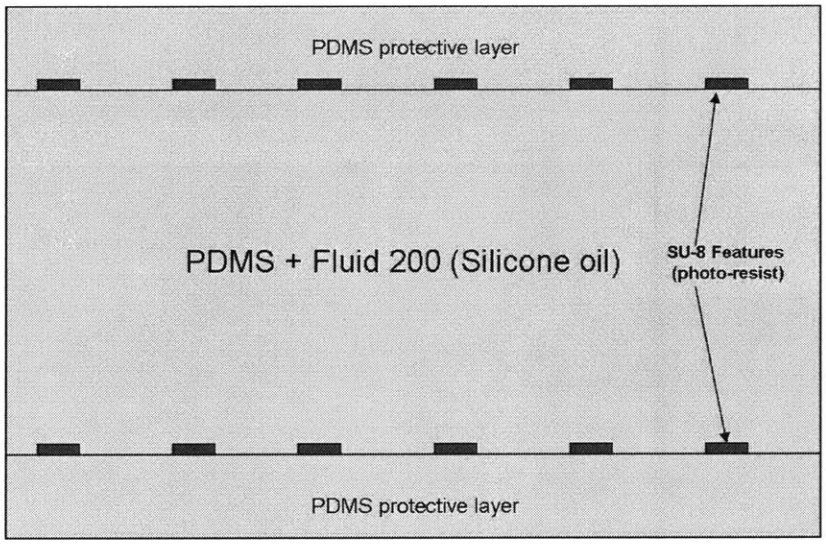

Figure 2.5: Design of the PDMS pressure sensor

The entire pressure sensor is transparent thus allowing the OCT to easily image structures within the Human Skin without hindrance from the pressure sensor. The OCT image will tell us the deformations of the features embedded within the pressure sensor. A continuum mechanics model would be developed (described in chapter 3) which would tell us the pressure distribution caused due to the deformations of the features.

2.5 Analytical modeling of the sensor using continuum mechanics

In this section we model the response of the pressure sensor to an unknown load. We are to determine the stress distribution that an unknown load exerts on the interface between the sensor and the finger. The OCT image would pick up the displacements of the features. We are to model the inverse problem where information is not complete.

We have a 2D matrix and we know the displacement of a few points within the matrix, we need to determine the stress distribution at one of the boundaries with this information. In order to solve an analytical model, we need to make certain simplifications. We use standard continuum mechanics assuming the features to be points within a PDMS matrix. The PDMS matrix is assumed to be linear elastic within the specified strains.

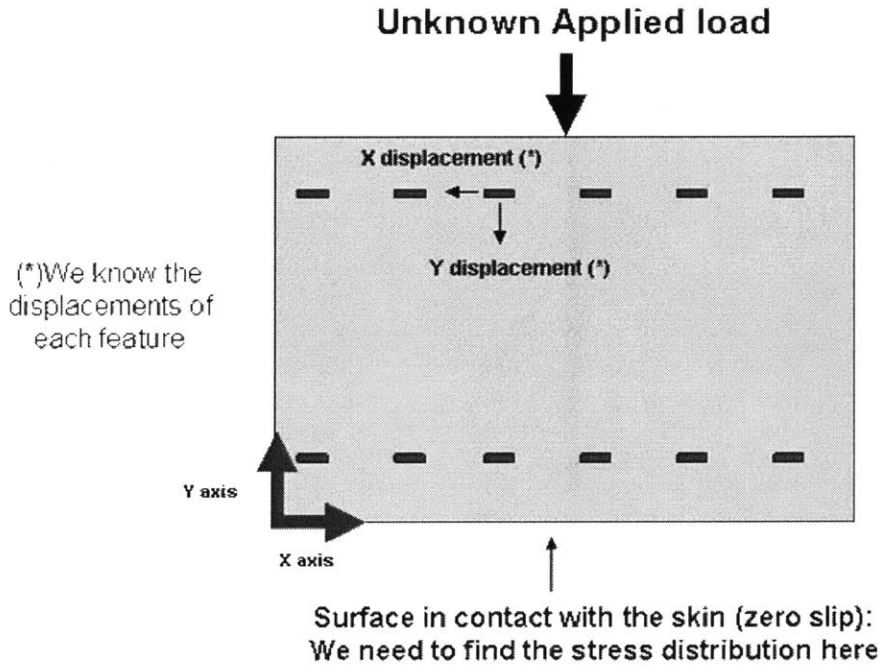

Figure 2.6: Geometric model of the sensor

In order to effectively model the sensor we model the strain field due to the motion of each bead. Since the displacements are small, we use will be small, we use the principle of superposition to get the net strain field at the bottom.

Chapter 3

Analytical Solution to the Inverse Problem

The working principle of the optical pressure sensor has been described in the previous section of this chapter. The bottom of the pressure sensor will be placed against the human finger. During our experiments, an unknown load will be incident on the top if the sensor. Due to this applied load, the features within the sensor will be displaced (refer to figure 2.6) and these displacements will be picked up by the OCT.

We are to determine the stress distribution at the bottom of the sensor (that part of the sensor that will be in contact with the finger) based on this information only. Thus, we have, in a way, incomplete strain information (or displacement information at a certain number of points within the matrix) and we are to determine the stress field based on this incomplete strain information and accompanying boundary conditions.

3.1 The Simplified "Bead" Model

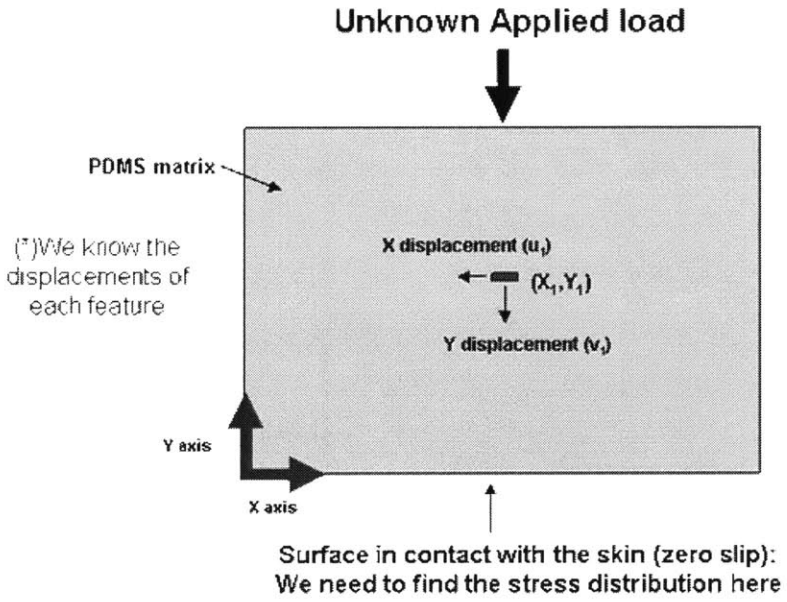

Figure 3.1: Simplified "bead" model of the sensor

In order to analytically solve this problem, we need to make certain simplifications. Instead of analyzing the motion of all the features together, we analyze the motion of each feature independently, determine the displacement field within the matrix due to the motion of each feature and then sum these displacement fields together to obtain the net displacement field. Since this is a linear system, the net strain field is also the sum of the individual strain fields.

The inverse problem can be thought of as the following.

Consider a 2D linearly elastic membrane of height h (along the y axis) with its bottom surface fixed to a stiff frame (which lay along the x axis). The rigid frame extends infinitely along the x axis and so does the 2D matrix. There is a bead embedded inside this matrix at coordinates (x1, y1) (refer to figure 3.1). We can control the motion of this bead. We displace this bead by a certain amount u1 (x displacement) and v1 (y displacement). The problem we need to solve is to determine the stress field at the bottom frame due to the motion of this one bead.

Thus, in the following derivations, we are given the displacements of this one bead. We need to find the strain field at the bottom of the sensor due to this displacement. We use the principle of superposition (described later in section 2.7.1) to find the net strain field at the bottom due to motion of all the beads. We use Equilibrium Equations, Constitutive Equations, and Compatibility Equations along with the Boundary conditions to get an analytic solution.

In the following derivations,

$\boldsymbol{\varepsilon}$ = strain tensor (2 dimensional) = $[\varepsilon_x\ \varepsilon_{xy};\ \varepsilon_{xy}\ \varepsilon_y]$

$\boldsymbol{\sigma}$ = stress tensor (2 dimensional) = $[\sigma_x\ \sigma_{xy};\ \sigma_{xy}\ \sigma_y]$

$\boldsymbol{\tau}$ = shear stress = σ_{xy}

$\boldsymbol{\Delta^2}$ = Laplace operator = $(\partial^2/\partial x^2 + \partial^2/\partial y^2)$

E = Young's Modulus

G = Shear Modulus

$\boldsymbol{\nu}$ = Poisson's Ratio

3.2 2D Equilibrium Equations

There are no external body forces:

- X Equilibrium:

$$\partial\sigma_x / \partial X + \partial\sigma_{xy} / \partial Y = 0 \quad \text{[1]}$$

- Y Equilibrium:

$$\partial\sigma_{xy} / \partial X + \partial\sigma_y / \partial Y = 0 \quad \text{[2]}$$

3.3 Constitutive Equations

For a linearly elastic isotropic medium, we have

$$\varepsilon_x = (1/E)[\sigma_x - \nu(\sigma_y + \sigma_z)] \quad \text{[3]}$$

$$\varepsilon_y = (1/E)[\sigma_y - \nu(\sigma_x + \sigma_z)] \quad \text{[4]}$$

$$\varepsilon_z = (1/E)[\sigma_z - \nu(\sigma_y + \sigma_x)] \quad \text{[5]}$$

$$\varepsilon_{xy} = (1/G)[\tau_{xy}] \quad \text{[6]}$$

- where

E- Young's Modulus

V- Poisson's Ratio

Our sensor extends indefinitely in the z direction thus $\varepsilon_z \sim 0$ (strain is negligible in the z direction), this leads to

$$\sigma_z = \nu(\sigma_y + \sigma_x) \quad \text{[7]}$$

Substituting back into equations [3] and [4], we get

$$\varepsilon_x = ((1+\nu)/E)[\sigma_x - \nu(\sigma_y + \sigma_x)] \quad \text{[8]}$$

$$\varepsilon_y = ((1+\nu)/E)\,[\sigma_y - \nu(\sigma_x + \sigma_y)] \quad \text{.....[9]}$$

3.4 Compatibility Equations

$$\partial^2\varepsilon_x/\partial Y^2 + \partial^2\varepsilon_y/\partial X^2 = 2[\partial^2\,\varepsilon_{xy}/\partial X\,\partial Y] \quad \text{..... [10]}$$

Combining the constitutive ([3]-[6]), compatibility [10] and equilibrium equations ([1]-[2]), we get

$$\Delta^2\,(\varepsilon_x + \varepsilon_y) = 0 \quad \text{.....[11]}$$

It is this Laplace equation that we need to solve to get our desired strain fields.

3.5 Boundary Conditions

The pressure sensor would be placed between the OCT head (along with the load) and the finger. We assume zero slip condition at this interface. Thus

$$u\,(x, 0) = 0 \quad \text{.....[12a]}$$

$$v\,(x, 0) = 0 \quad \text{.....[12b]}$$

Where,

u is the X displacement of the bead withing the matrix

v is the Y displacement of the bead within the matrix (refer to fig 3.1)

Another boundary condition is zero strain far from the incident loading. In the following solution we assume this occurs at a distance **w** from the incident load. Thus,

$$\varepsilon_x (x1-w, y) = 0 \quad \text{.....[13]}$$

$$\varepsilon_y (x1-w, y) = 0 \quad \text{.....[14]}$$

We also have information of the motion of a bead within the matrix. Thus,

$$u(x1, y1) = u1 \quad \text{.....[15]}$$

$$v(x1, y1) = v1 \quad \text{.....[16]}$$

We also use symmetry conditions.

3.6 General Solution to the Laplace equation

In order to get an analytical solution of the problem described above, we need to solve the Laplace equation derived in equation [11],

$$\Delta^2 (\varepsilon_x + \varepsilon_y) = 0.$$

Let us analyze the Laplace equation

$$\Delta^2 \Phi(x, y) = 0 \quad \text{.....[17]}$$

We reduce the partial differential equation to a set of ordinary differential equations by separating variables.

$$\Phi(x, y) = X(x)\, Y(y)$$

Where, X(x) and Y(y) are functions of x only and y only respectively.

Substituting back in **[12]**, we get

$$\Delta^2 \Phi(x, y) = (\partial^2\Phi / \partial x^2 + \partial^2\Phi / \partial y^2)$$
$$= (1/X)\,(\partial^2 X / \partial x^2) + (1/Y)\,(\partial^2 Y / \partial y^2) = 0$$

Since x and y are independent, we get

$$(\partial^2 X / \partial x^2) = \lambda^2 X \quad \text{..... [18]}$$

$$(\partial^2 Y / \partial y^2) = -\lambda^2 Y \quad \text{..... [19]}$$

Where λ is a constant

The general solution to the above equations has the form:

$$Y(y) = \alpha \cos(\lambda y) + \beta \sin(\lambda y) \quad \text{..... [20]}$$
$$X(x) = \gamma \cosh(\lambda x) + \delta \sinh(\lambda x) \quad \text{..... [21]}$$

Where $\alpha, \beta, \gamma, \delta$ are constants

Thus we use the above solutions to determine the strain field subject to the boundary conditions described in

3.7 Simplifying the problem using the principle of superposition

In order to use the Laplace solution described in the previous section, we will need to make a few more simplifications to our model described in section 3.1. We first assume that the feature is a point within the matrix. An unknown load applied to the matrix causes this feature to move within the matrix. We know the x and y displacement of this one bead. We now decompose this problem into two problems using the principle of superposition. The net displacement field due to the x and y motion is the sum of the displacement field due to the x motion and that due to the y motion of the bead. Since this is a linear system, we can say the same for the strain field. This is described in figure 3.2.

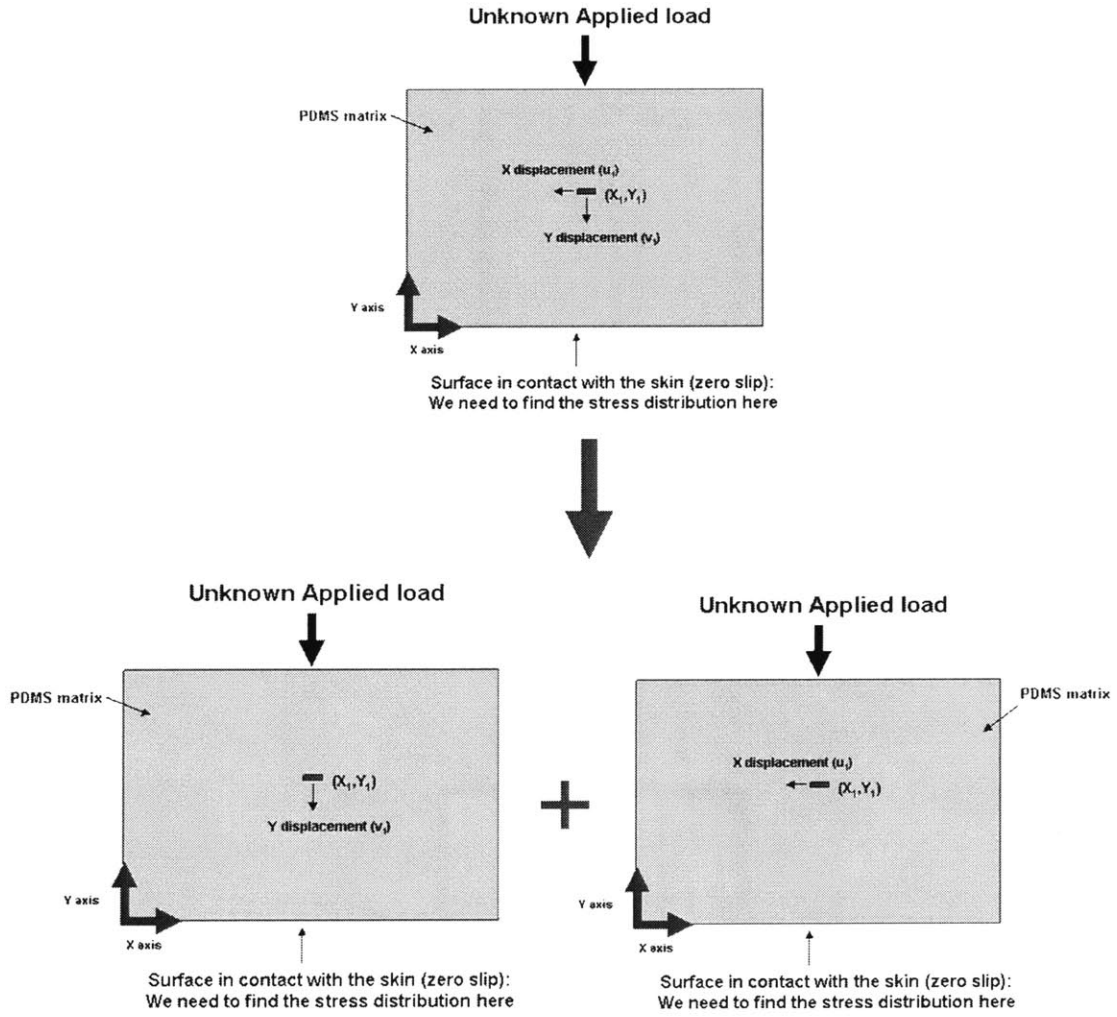

Figure 3.2: Figure illustrating the Principle of Superposition applied to the sensor to simplify the problem.

3.7.1 Analysis of Y displacement

We first analyze the Y displacement only. We know the y displacement and need to determine the displacement fields: u(x, y) and v(x, y) due to this motion.

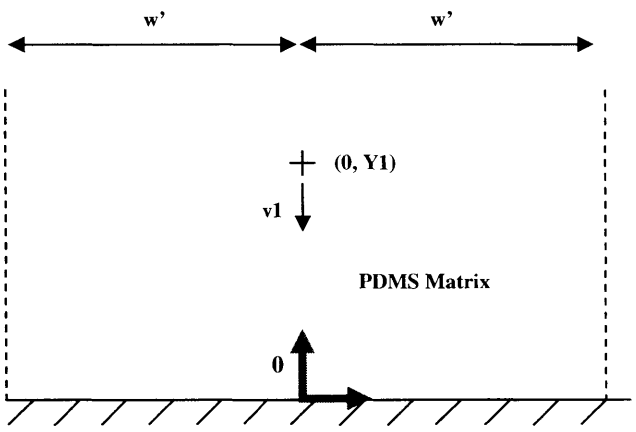

Figure 3.3: Figure illustrating the Y motion of the bead embedded in a PDMS matrix

As mentioned in section 3.4, we have to solve $\Delta^2 (\varepsilon_x + \varepsilon_y) = 0$ subject to the boundary conditions. In this simplified version, we assume that we have a bead (point) embedded in a PDMS matrix. The bottom of the matrix is fixed to a rigid frame (hashed line in figure 3.3). We move this point down a vertical distance v1. We now have to determine the displacement field within the matrix due to this motion.

In this case it is to be noted that $\varepsilon_x << \varepsilon_y$. As we assume the bead to be a point, the strain in the x direction due to this vertical motion is very small as compared to the strains in the y direction. Thus the Laplace equation simplified to

$$\Delta^2 (\varepsilon_y) = 0 \quad \text{..... [22]}$$

The boundary conditions are (referring to section 3.5).

$$v = 0 \text{ for all } (x, 0) \quad \text{..... [23]}$$

$$v = -v1 \text{ at } (0, y1) \quad \text{..... [24]}$$

$$\varepsilon_y = 0 \text{ at } (-w', y) \text{ and } (w', y) \text{ ..... [25]}$$

Equation [25] suggests that at x = -w'/2, the strains are zero for all y. Thus this is a strain free edge (represented by the dotted line in figure 3.3). This boundary condition and the value of w' is determined by observing images of the undeformed and deformed images and determining an edge where no effect of the incident load is transmitted. This will be illustrated in chapter 5 where a description of the image processing would be discussed. Strain is also 0 at x = w'/2 for all y due to symmetry conditions.

Assuming variable separation we get

$$\varepsilon_y(x, y) = X(x)\, Y(y)$$

and from Eq. [20] and [21] we get,

$$X(x) = \alpha \cos(\lambda x) + \beta \sin(\lambda x) \text{ ..... [26]}$$
$$Y(y) = \gamma \cosh(\lambda y) + \delta \sinh(\lambda y) \text{ ..... [27]}$$

Applying Boundary condition [25]

$$\varepsilon_y(-w', y) = [\alpha \cos(-\lambda w') + \beta \sin(-\lambda w')]\, [\gamma \cosh(\lambda y) + \delta \sinh(\lambda y)] = 0$$
(Constant) (Variable)

This is true for all y, thus

$$\alpha \cos(-\lambda w') + \beta \sin(-\lambda w') = 0$$
$$\alpha \cos(\lambda w') = \beta \sin(\lambda w') \text{ ..... [28]}$$

Applying the other boundary condition,

$$\varepsilon_y(w', y) = [\alpha \cos(\lambda w') + \beta \sin(\lambda w')]\, [\gamma \cosh(\lambda y) + \delta \sinh(\lambda y)] = 0$$
(Constant) (Variable)

This is also true for all y, thus

$$\alpha \cos(\lambda w') + \beta \sin(\lambda w') = 0 \text{ , or}$$

$$\alpha \cos(\lambda w') = -\beta \sin(\lambda w') \quad \ldots\ldots [29]$$

From [28] and [29] , we get

$$\beta = 0 \text{ and}$$

$$\lambda = [(n+1)\pi] / [2*w'] \quad \ldots\ldots [30]$$

Thus the strain reduces to

$$\varepsilon_y(x, y) = [\alpha \cos(\lambda x)] [\gamma \cosh(\lambda y) + \delta \sinh(\lambda y)]$$

or

$$\varepsilon_y(x, y) = [\cos(\lambda x)] [\gamma' \cosh(\lambda y) + \delta' \sinh(\lambda y)] \quad \ldots\ldots [31]$$

We now have to solve for two unknowns γ' and δ'.

Let ε_{y1} be the strain at (0, Y1). We will determine its value later. This will be our next boundary condition.

$$\varepsilon_y(0, Y1) = \varepsilon_{y1} = [\gamma' \cosh(\lambda Y1) + \delta' \sinh(\lambda Y1)] \quad \ldots\ldots [32]$$

We need one more boundary condition to completely solve this equation. As has been explained earlier, in our "bead" model, we apply the y displacement (v1) to the bead to simulate the motion of the beads due to the incident loads. Thus as the motion of the bead causes the most displacement of the matrix at (0, Y1), $\varepsilon_y(0, Y1)$ is a max at (0, Y1). Thus,

$$\partial\varepsilon_y(0, Y1)/\partial y = 0 \text{ at } (0, Y1) \quad \ldots\ldots [33]$$

This gives us,

$$\partial \varepsilon_y (0, Y1)/ \partial y = \lambda [\gamma' \sinh (\lambda Y1) + \delta' \cosh (\lambda Y1)] = 0$$

Thus,

$$[\gamma' \sinh (\lambda Y1) + \delta' \cosh (\lambda Y1)] = 0 \quad \text{[34]}$$

Solving [32] and [34] we get the values of γ' and δ'

$$\gamma' = \varepsilon_{y1} / [\gamma' \cosh (\lambda Y1) + \tanh (\lambda Y1) \sinh (\lambda Y1)] \quad \text{[35]}$$

$$\delta' = \tanh (\lambda Y1)\, \gamma' \quad \text{[36]}$$

We now have the expression of $\varepsilon_y(x, y)$; we still have to find the value of ε_{y1} in terms of the y displacement v1. We integrate equation [31] with respect to y and use the boundary condition that the displacement is 0 at the bottom (no slip at the bottom rigid frame).

$$v (x, y) = \int (\partial \varepsilon_y(x, y)/ \partial y)\, dy = [\cos (\lambda x)/ \lambda] [\gamma' \sinh (\lambda y) + \delta' \cosh (\lambda y)] + F(x)$$

Now, $v (x, 0) = 0$, thus

$$F(x) = - [\cos (\lambda x)/ \lambda] \delta'$$

Thus,

$$v (x, y) = [\cos (\lambda x)/ \lambda] [\gamma' \sinh (\lambda y) + \delta' \cosh (\lambda y)] - [\cos (\lambda x)/ \lambda] \delta'$$

Also,

$$v (0, Y1) = -v1 \text{ (displacement of bead)}$$

$$v (0, Y1) = [\cos (0)/ \lambda] [\gamma' \sinh (\lambda Y1) + \delta' \cosh (\lambda Y1)] - [\cos (0)/ \lambda] \delta' \quad \text{[37]}$$

Solving this and [36] we get,

$$\gamma' = -\lambda\, v1/[2 \sinh(\lambda Y1) - \tanh(\lambda Y1)] \quad \text{.....[38]}$$

$$\text{with } \delta' = \tanh(\lambda Y1)\, \gamma'$$

This is the model for the y displacement field due to only y motion of the bead

3.7.2 Analysis of X displacement

We now analyze the deformation of the bead in the matrix when the bead is moved along the x axis only. We use boundary conditions along with the Laplace equation to determine the strain field in the x direction.

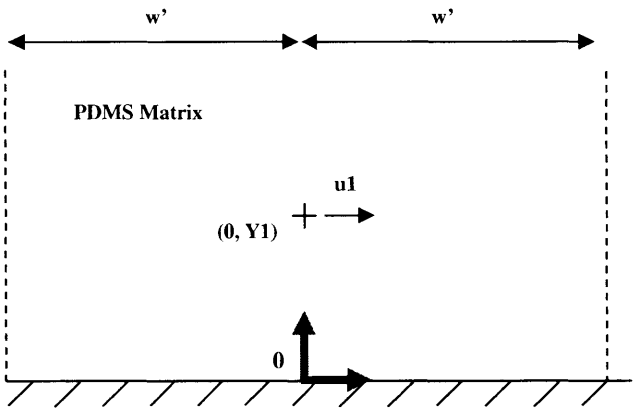

Figure 3.4: Figure illustrating the X motion of the bead embedded in a PDMS matrix

In this case too, as before, we are given the displacements of the bead within the matrix and we are to determine the stress at the bottom frame due to the motion of this bead. We have to solve

$$\Delta^2 (\varepsilon_x + \varepsilon_y) = 0$$

In this case it is to be noted that $\varepsilon_x >> \varepsilon_y$. As we assume the bead to be a point, the strain in the y direction due to this horizontal motion is very small as compared to the strains in the x direction. Thus the Laplace equation simplified to

$$\Delta^2 (\varepsilon_x) = 0 \quad \text{..... [39]}$$

The boundary conditions are

$$u = 0 \text{ for all } (x, 0) \quad \text{..... [40]}$$

$$u = u1 \text{ at } (0, y1) \quad \text{..... [41]}$$

$$\varepsilon_y = 0 \text{ at } (-w', y) \text{ and } (w', y) \quad \text{..... [42]}$$

As before, x = **-w'** and **w'** is a strain free edge (represented by the dotted line in figure 3.4). This boundary condition and the value of w' is determined by observing images of the undeformed and deformed images and determining an edge where no effect of the incident load is transmitted.

Assuming variable separation we get

$$\varepsilon_x(x, y) = X(x)\, Y(y)$$

and from Eq. [20] and [21] we get,

$$X(x) = \alpha 1 \cos(\lambda 1\, x) + \beta 1 \sin(\lambda 1\, x) \quad \text{..... [43]}$$

$$Y(y) = \gamma 1 \cosh(\lambda 1\, y) + \delta 1 \sinh(\lambda 1\, y) \quad \text{..... [44]}$$

Applying Boundary condition [25]

$$\varepsilon_x(-w', y) = [\alpha 1 \cos(-\lambda 1\, w') + \beta 1 \sin(-\lambda 1\, w')]\, [\gamma 1 \cosh(\lambda 1\, y) + \delta 1 \sinh(\lambda 1\, y)] = 0$$

(Constant) **(Variable)**

This is true for all y, thus

$$\alpha 1 \cos(\lambda 1\, w') + \beta 1 \sin(-\lambda 1\, w') = 0$$

$$\alpha 1 \cos(\lambda 1\, w') = \beta 1 \sin(\lambda 1\, w') \quad \text{..... [45]}$$

Applying the other boundary condition,

$$\varepsilon_x(w', y) = [\alpha 1 \cos(\lambda 1\, w') + \beta 1 \sin(\lambda 1\, w')]\, [\gamma 1 \cosh(\lambda 1\, y) + \delta 1 \sinh(\lambda 1\, y)] = 0$$

(Constant) **(Variable)**

This is also true for all y, thus

$$\alpha 1 \cos(\lambda 1\, w') + \beta 1 \sin(\lambda 1\, w') = 0 \text{ , or}$$

$$\alpha 1 \cos(\lambda 1\, w') = -\beta 1 \sin(\lambda 1\, w') \quad \text{..... [46]}$$

From these we get,

$$\beta 1 = 0 \text{ and}$$

$$\lambda 1 = [(n+1)\,\pi] / [2*w'] \;\ldots\ldots\ldots\ldots\ldots\ldots\ldots\ldots\ldots\ldots\ldots\ldots\ldots\ldots \;[47]$$

Thus the strain reduces to

$$\varepsilon_x(x, y) = [\alpha 1 \cos(\lambda 1\, x)]\,[\gamma 1 \cosh(\lambda 1\, y) + \delta 1 \sinh(\lambda 1\, y)]$$

or

$$\varepsilon_x(x, y) = [\cos(\lambda 1\, x)]\,[\gamma 1' \cosh(\lambda y) + \delta 1' \sinh(\lambda y)] \;\ldots\ldots\; [48]$$

We now have to solve for two unknowns **$\gamma 1'$** and **$\delta 1'$** to get a solution to the Laplace equation.

Let ε_{x1} be the strain at (0, Y1). We will determine this value later using **[12a]**. This will be our next boundary condition.

$$\varepsilon_x(0, Y1) = \varepsilon_{x1} = [\gamma 1' \cosh(\lambda 1\, Y1) + \delta 1' \sinh(\lambda 1\, Y1)] \;\ldots\ldots [49]$$

We need one more boundary condition to completely solve this equation. As has been mentioned earlier, in our "bead" model, we apply the y displacement (v1) to the bead to simulate the motion of the beads due to the incident loads. Thus as the motion of the bead causes the most displacement of the matrix at (0, Y1), ε_x **(0, Y1)** is a max at (0, Y1). Thus,

$$\partial \varepsilon_x (0, Y1) / \partial x = 0 \text{ at } (0, Y1) \;\ldots\ldots\ldots\ldots\ldots\ldots\ldots\ldots\ldots\ldots\ldots \;[50]$$

This gives us,

$$\partial \varepsilon_y (0, Y1) / \partial y = \lambda 1 \sin(\lambda 1\; 0)\;\; [\gamma' \sinh(\lambda Y1) + \delta' \cosh(\lambda Y1)] = 0$$

This is always valid, thus cannot be used by us as a boundary condition, we have to find another boundary condition to determine another equation.

Now,

$$\varepsilon_x(x, y) = [\cos(\lambda 1\, x)]\,[\gamma 1' \cosh(\lambda y) + \delta 1' \sinh(\lambda y)] = \partial u(x, y)/\partial x$$

Thus,

$$u(x, y) = [-\sin(\lambda 1\, x)/\lambda 1]\,[\gamma 1' \cosh(\lambda y) + \delta 1' \sinh(\lambda y)] + F'(y) \quad \text{....[51]}$$

using **[12a]**, the displacement field at the bottom is 0

$$u(x, 0) = [-\sin(\lambda 1\, x)/\lambda 1]\,[\gamma 1'\,] + F'(0)$$

this is true for all x thus,

$$\gamma 1' = 0 \text{ and } F'(0) = 0 \quad \text{.....[52]}$$

thus

$$u(x, y) = [-\sin(\lambda 1\, x)/\lambda 1]\,[\,\delta 1' \sinh(\lambda y)] + F'(y) \quad \text{.....[53]}$$

From [49]

$$\varepsilon_{x1} = [\,\delta 1' \sinh(\lambda 1\, Y1)]$$

thus

$$\delta 1' = \varepsilon_{x1} / \sinh(\lambda 1\, Y1) \quad \text{..... [54]}$$

We use the fact that the left edge of the figure is stain and displacement free.

Thus,

$$u(-w', y) = [-\sin(\lambda 1\, w')/\lambda 1]\,[\,\delta 1' \sinh(\lambda y)] + F'(y) = 0$$

$$F'(y) = [1/\lambda 1]\,[\,\delta 1' \sinh(\lambda y)] \quad \text{.....[55]}$$

It is to be noted that [55] satisfies [52] as well, thus this solution is consistant.

Thus finally we get,

$$\mathbf{u\ (x, y) = [-\sin (\lambda 1\ x)/\ \lambda 1]\ [\delta 1'\ \sinh (\lambda y)] + [1/\ \lambda 1]\ [\ \delta 1'\ \sinh (\lambda y)]....[56]}$$

Where, **$\delta 1'$** is defined by [54]

We still need to determine ε_{x1} in terms if u1 to complete the solution.

$$\mathbf{U(0,Y1) = u1 = [1/\ \lambda 1]\ [\ \delta 1'\ \sinh (\lambda Y1)]}$$

$$\mathbf{\delta 1' = (u1\ \lambda 1)/\ \sinh (\lambda Y1).....[57]}$$

Combining [54] and [57], we get

$$\varepsilon_{x1} = \mathbf{u1\ \lambda 1.....[58]}$$

This completes the model.

3.8 Model summary

The displacement fields are defined by

$$\mathbf{u\ (x, y) = -D_x\ (\sin (k*x)/\ k)\ \sinh (h*y) + (D_x/k)\ \sinh (k*y)}$$
$$\mathbf{v(x, y) = (\cos (k*x)\ /\ k)\ (C_y\ \sinh (k*y) + D_y\ \cosh (k*y) - D_y)}$$

Where,

$\mathbf{Cy = -(k*\ v1)/[2\ *\sin (k*y1) - \tanh (k*y1)]}$
$\mathbf{Dy=C'\ \tanh (k*y1)}$
$\mathbf{D_x = (k*\ u1)/\sinh (k*y1)}$
$\mathbf{k = [(n+1)\ \pi]\ /\ [2*w']}$

This displacement field is due to the motion of one bead. The net displacement field is obtained by the summation of the displacement fields due to each of the features. This is then used to compute the strain field and stress fields at the interface.

Chapter 4

Fabrication

As mentioned in section 2.2, the design of the sensor requires it to be flexible; near transparent and the total device thickness is to be 150 microns. To meet these requirements, we use soft lithography techniques to manufacture the sensor using the transparent polymer PDMS. The entire device is fabricated bottom up on a silicon wafer using soft lithography techniques. A brief description of the manufacturing process as well as apparatus used is described below.

4.1 Soft Lithography

Photolithography is the most successful technology in micro fabrication since its invention in 1959 [26]. It is widely used in the semiconductor industry to manufacture integrated circuits. However, these techniques do have some limitations; feature sizes in photolithography are limited by optical diffraction and the accompanying apparatus is expensive and complicated. Further these techniques cannot be applied to non planar surfaces. Soft lithography techniques were developed by Xia et al [27] to circumvent some of the limitations of photolithography. Soft lithography techniques provide a set of methods that enable the manufacture of high-quality patterns and structures with lateral dimensions of about 30 nm to 500 μm.

We will employ these techniques to generate features over a PDMS substrate. First a brief introduction to the various steps as well as the accompanying apparatus is presented; this will be followed by a description of the features generated and problems encountered.

4.2 Fabrication Overview

We use a silicon wafer as the substrate on which we manufacture the sensor. The basic fabrication steps involved are spin coating of the polymer over the silicon wafer, spin coating of the photo resist over the polymer film, UV exposure of the photo resist using a photomask containing the features and finally development of the features using the appropriate developer solution and finally coating the features again with PDMS. This procedure of repeated twice to generate the 5 layer device. A schematic of the procedure is depicted in figure 4.1. A brief description of the process steps follows.

4.2.1 Spin Coating

Spin coating is a technique widely used for the application of thin films onto substrates. The process involves the deposition of a small puddle of the fluid/resin (in our case PDMS and later the photo resist) in the middle of the substrate (in our case a 4 inch silicon wafer). The substrate is then spun at a very high speed. The centripetal acceleration causes the resin to spread over the circular substrate and leave a thin film of the resin on the surface of the substrate. The speed at which the substrate is spun as well as the time during which the substrate spins determines the thickness of the film deposited over the Si substrate.

For our process, A Si substrate was cleaned with acetone and isopropyl alcohol. Before the wafer is placed on the chuck of the spin coater, it is silanized (passivation of the surface to make it not stick to the PDMS) with a silanizing agent (tridecafluoro-1,1,2,2-tetrahydrooctyl trichlorosilane) in a vacuum degasser. This prevents the polymer from

strongly adhering to the Si substrate as the entire wafer needs to be peeled from the substrate after the process is complete.

In a separate container, PDMS is mixed in the ratio 1:10, was degassed and dispensed onto the silanized Si substrate. For this first layer of PDMS (refer to figure 4.1), the substrate was spun at 500 rpm for 15 seconds and then the speed was ramped up to 2500 rpm for 30 seconds. This led to a thickness of 25 microns. The substrate was then placed in a 65 degree oven for 2 hours to dehydrate and crosslink.

The dried substrate is placed back onto the spin coater and is dispensed with the photo resist and the spin coating process is repeated. The photo resist selected for the process was AZ4620 (from MicroChem corp., Newton MA). We will later use the epoxy based negative photo resist SU-8 in our process and will explain the reasons for doing so.

AZ4620 was dispensed on the substrate and spun at 500 rpm for 15 seconds followed by 2000 rpm for 30 seconds. This leads to a thickness of around 10 microns. This is left to dry on a hot plate at 65 degrees for 10 minutes.

4.2.2 UV Exposure and Development

In order to create features on the PDMS and silicon substrate, the photo resist film needs to be exposed and developed. Photo resists are most commonly used at wavelengths in the ultraviolet spectrum or shorter (<400 nm). As we are using a positive photo resist, the portion of the photo resist that is exposed to the UV light becomes soluble to the photo resist developer and the portion of the photo resist that is unexposed remains insoluble to the photo resist developer.

We use a photomask with the required pattern on it to pattern the photo resist. The Exposure is done on a Karl Zeiss aligner. We expose of the dried photo resist (from the hot plate) to UV radiation using a mask aligner as shown in figure 4.1.

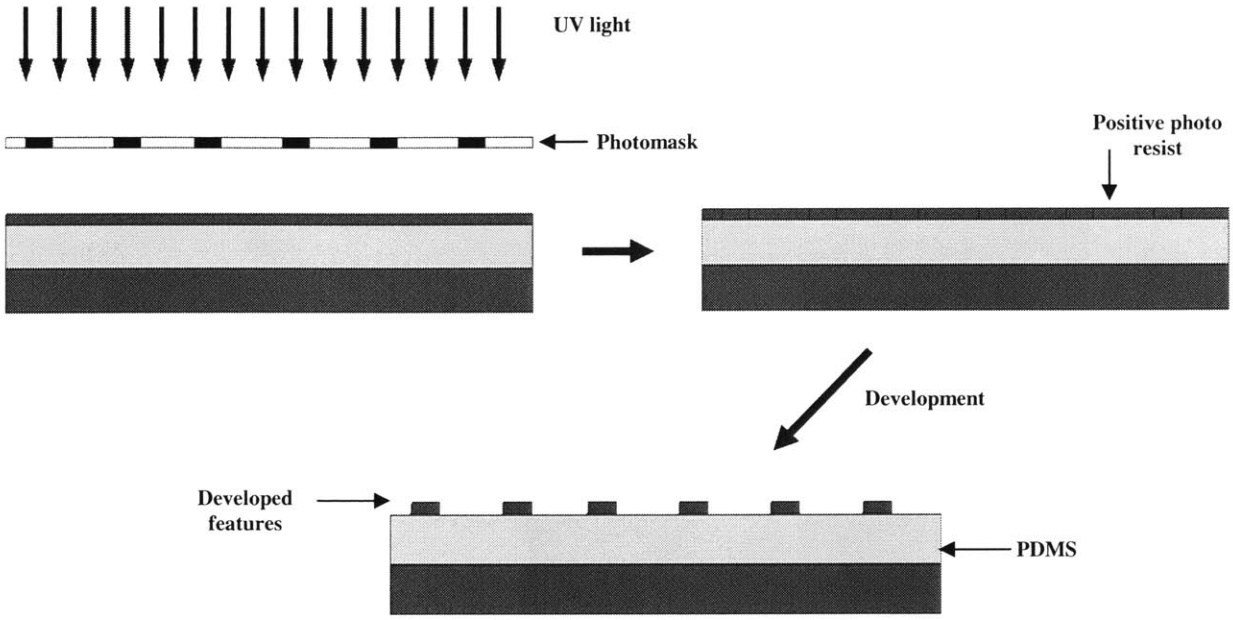

Figure 4.1: Schematic describing the UV exposure and Development of the photo resist on the PDMS substrate

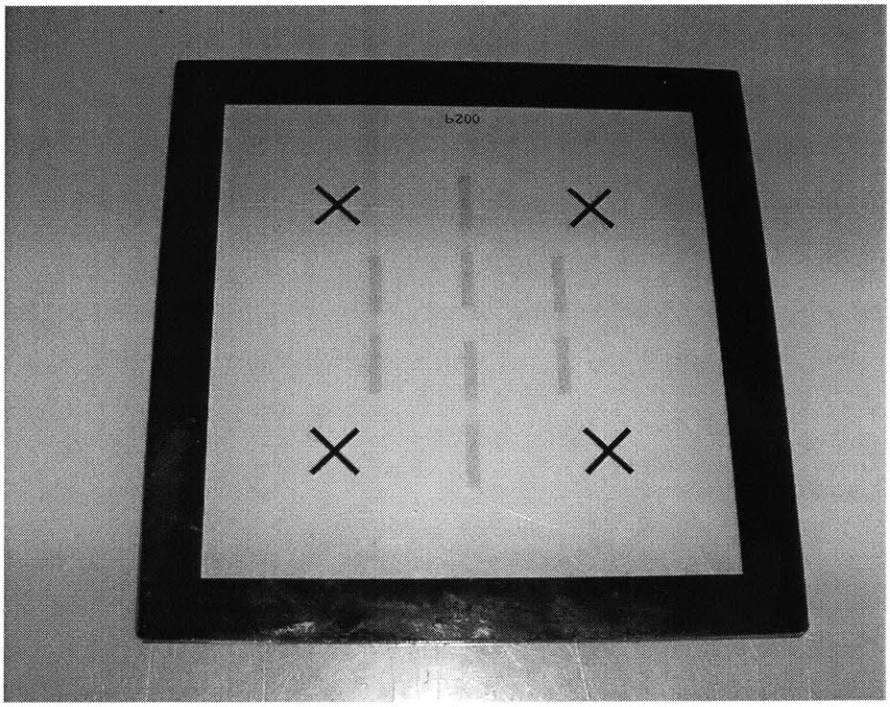

Figure 4.2: Photomask (Bright field) used to manufacture the sensor

The wafer was exposed for 30 seconds in 10 second bursts keeping a relax time of 10 seconds between bursts. After which the wafer was developed in AZ440 for 2 minutes.

This is followed by spin coating another layer of PDMS on the developed features at 700 rpm for 45 seconds. This bought the thickness of the middle PDMS layer to 80 microns. The wafer is then soft baked in the oven for 2 hours to let the PDMS cure.

Another layer of photo resist is then coated on this followed by exposure and development. Before the exposure, the photomask is carefully aligned so as to overlap the features on the second layer this is done by matching the alignment marker of the photomask to the developed alignment mark on the second layer of the device. This ensures that the features on the second and fourth layer of the device are aligned.

Finally the last layer of PDMS is coated (500 rpm for 15 seconds followed by 2500 rpm for 30 seconds) completing the 5 layer device. The entire device is then placed in the soft bake oven for 2 hours. The entire device is then carefully peeled off the silicon wafer.

4.3 Problems with the AZ4620 sensor

The major problem faced with the AZ4620 sensor was of the lack of adhesion of the photo resist to the PDMS. After the exposure of the photo resist layer, after development the AZ4620 features float of the PDMS substrate due to poor adhesion.

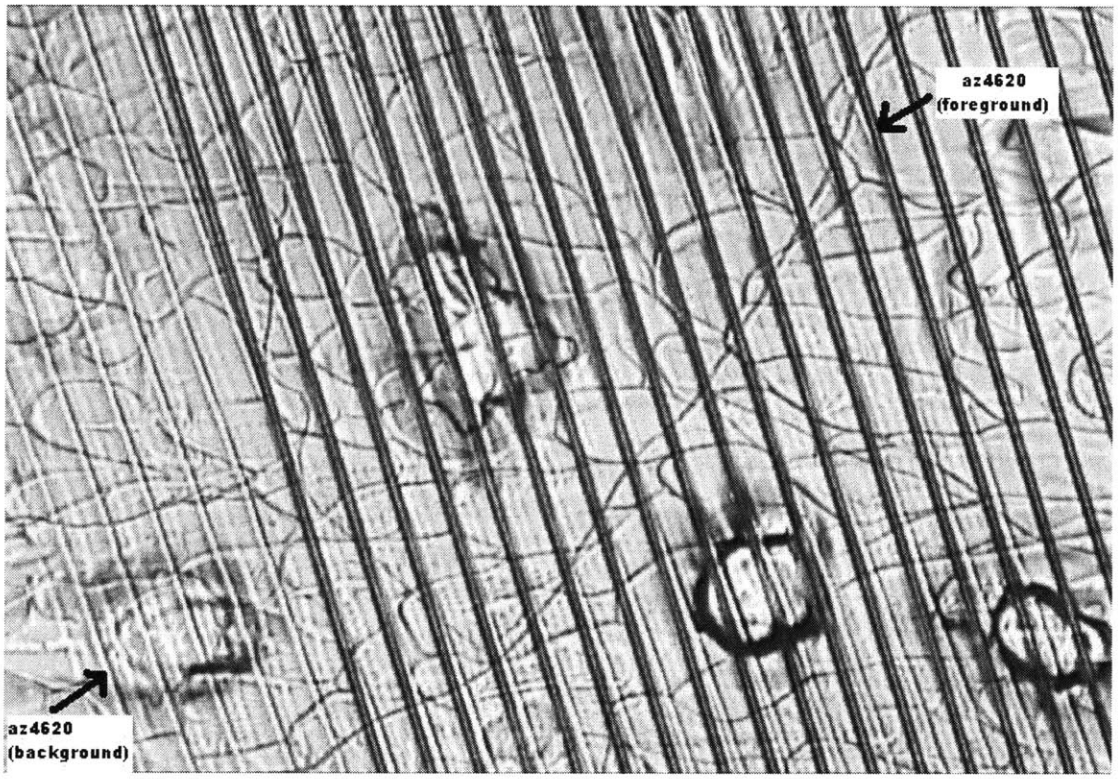

Figure 4.3: A top down view of the completed AZ4620 sensor showing the top and bottom features. Due to a misalignment error the features are not aligned properly (the separation of the features (parallel bars) is 100 microns). Note: the entire sensor has a reddish tinge (with cracks) to it due to a very thin layer of AZ4620 deposited over the entire 1st and 3rd layer of PDMS.

The photo resist is found to adhere to the PDMS substrate only when there is a thin layer of photo resist accompanying the feature (see figure 4.3). Another problem encountered was during the final step of peeling the sensor from the silicon wafer.

When the sensor is peeled off the Si wafer, the layers of the photo resist separate from the top and bottom PDMS layers of the device thus leaving us with three separate layers. In order to improve the adhesion, HMDS solution (an adhesion promoter) was applied to the

PDMS substrate before spin coating the photo resist. However, the adhesion problem still remained.

In addition to this there was the problem of cracking of the thin film of AZ4620 (refer to figure 4.3). This would lead to distortions in images obtained when used with the OCT.

In order to circumvent these problems, it was decided to use another photo resist which was more compatible with the PDMS substrate and employ another technique to further strengthen the bond between PDMS and the photo resist.

We use the negative photo resist SU-8 which has better adhesion properties than AZ4620. We find that the resist SU-8 2100 is best suited for our purpose as it has the best adhesion to PDMS substrate. But the problem of wetting still remains. During the pre-exposure bake step of the SU-8 (refer to figure 4.4), it is found that the photo resist film tends to contract thus not completely wetting the PDMS substrate. We need to introduce another process step to improve the wetting of SU-8 to PDMS.

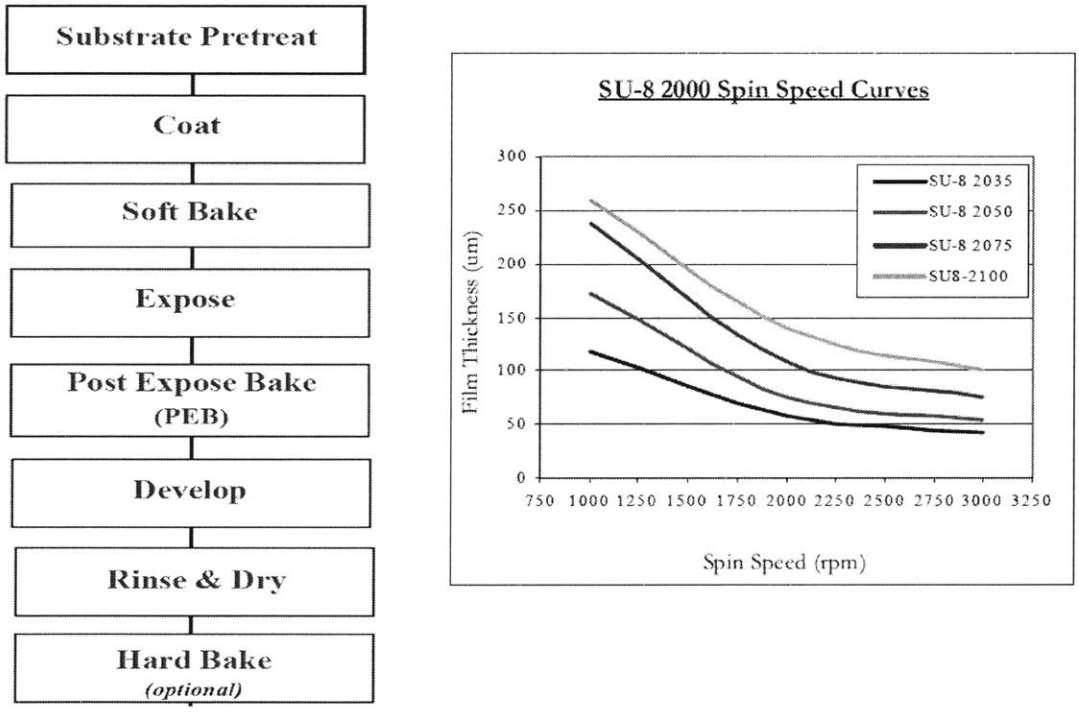

Figure 4.4: SU-8 process steps and spin speed parameters (MicroChem ® nano SU-8 2000 data sheet)

4.4 Oxygen Plasma to enhance adhesion and wetting

In order to increase the wetting and adhesion of the photo resist on PDMS, we expose the surface of PDMS to oxygen plasma for varying times. PDMS is hydrophobic by nature, but exposure to oxygen plasma increases the surface energy of the polymer, increasing the wetting of photo resist on the polymer (making it hydrophilic). We use a goniometer to measure the contact angle of a drop of distilled water on the PDMS surfaces exposed to oxygen plasma for different times.

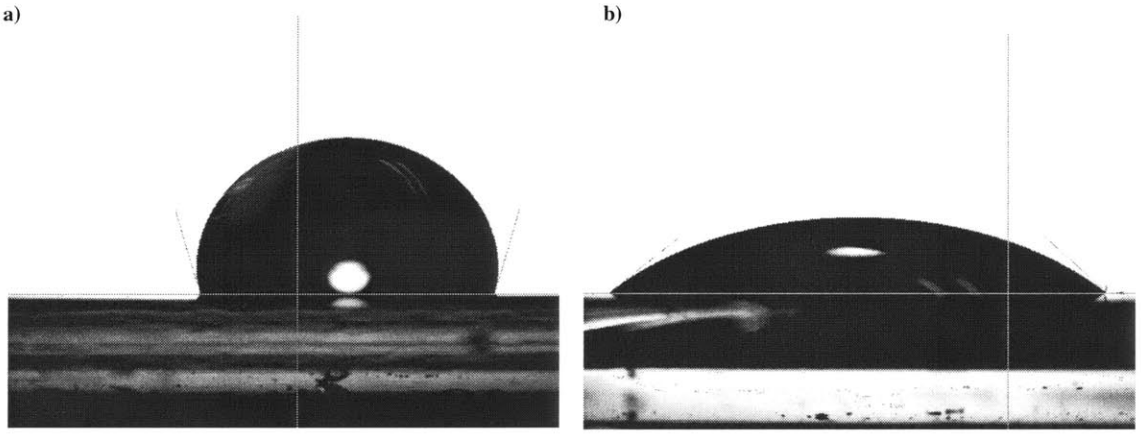

Figure 4.5: Figure showing the change in wetting of a drop of distilled water on PDMS on exposure to oxygen plasma a) unexposed (contact angle 110 °) and b) Exposed to Oxygen plasma for 3 seconds (contact angle 38.7°)

In addition to this we also study the recovery of the PDMS surface to its original state after exposure to Oxygen plasma. PDMS samples (mixed in the ratio 1:10) were prepared on glass slides and soft baked for 2 hours to cure.

The samples were then exposed to oxygen plasma for 2, 4, 6, 12 and 15 seconds respectively. The samples were kept in the open (exposed to the atmosphere) and contact angle measurements were made periodically on the goniometer.

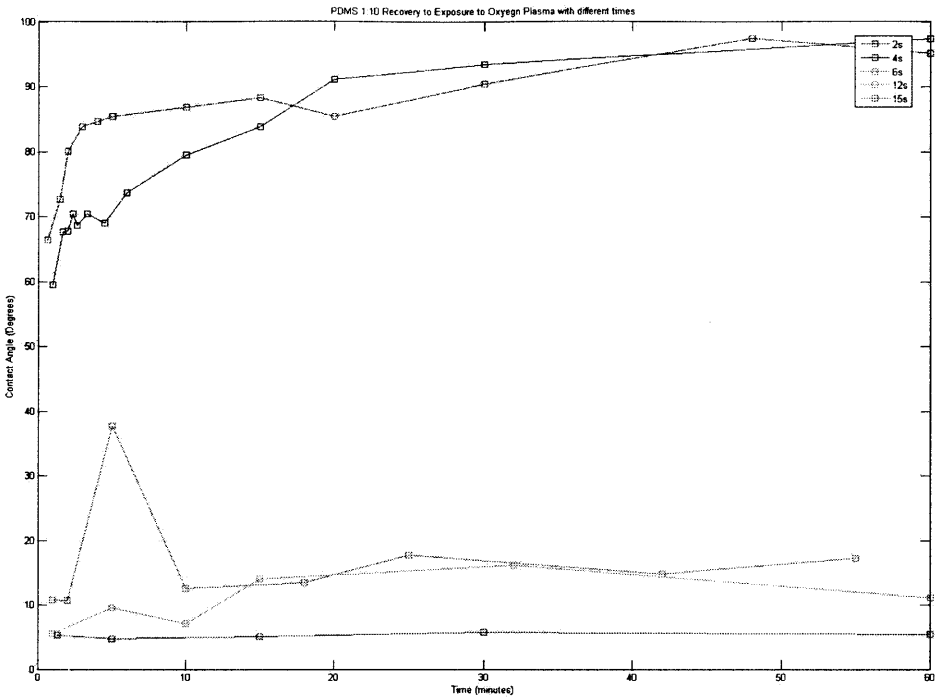

Figure 4.6: PDMS recovery to exposure to Oxygen plasma. It was found that if exposure was below 6 seconds, the sample recovered to close to its original hydrophobicity within an hour

It was found that there exists an exposure time limit above which the PDMS surface took a long time to recover. Below this limit the PDMS recovered to its original hydrophobicity within an hour. The limit was found to be 6 seconds.

When the sample was exposed above 6 seconds, the hydrophobicity didn't return for days. Measurements were taken up to a time of 5 days and the recovery still wasn't significant.

We now include the exposure of PDMS to oxygen plasma in our process steps before spin coating on the photo resist.

4.5 Fabrication of negative photomask

We would use the negative photo resist SU-8 2100 in our process. A negative resist is a type of photo resist in which the portion of the photo resist that is exposed to light becomes relatively insoluble to the photo resist developer. The unexposed portion of the photo resist is dissolved by the photo resist developer. As in this case the wafer image would be opposite to the mask image, we would not be able to use the photo mask we used earlier. We would need to reverse the mask from a bright field mask to a dark field mask (its complement). We use the positive resist AZ5214 to do so.

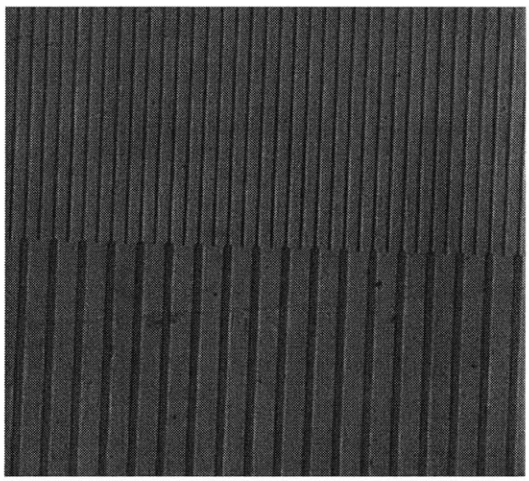

Figure 4.7: Negative photomask manufactured for the negative Photoresist SU-8 by wet etching. The distance between the parallel thick bars is 100 microns

The recipe for mask reversal using AZ5214 is as follows. We start off with spin coating 2 microns of this resist onto a chromium coated glass plate. The plate is then soft baked at 90^{o} for 25 minutes. This is now exposed to UV light using the High Resolution aligner using a back filter for 20 seconds. The original photomask is used as the mask for this step. The resist is allowed to cross link by baking it in the 90 o oven for 30 minutes. The plate is now "flood" exposed on the High Resolution aligner without the back filter and without the mask for 1 minute. The AZ5214 is then developed using the AZ422 developer. The plate is then wet etched using CR-7 for about 40 seconds. The plate is

then distilled using distilled water. An image of the manufactured mask is depicted in figure 4.7

4.6 Summary of process steps

A thin layer (of about 20 microns) of PDMS mixed to a ratio of 1:10 (curing agent to PDMS) is spin coated on a clean silicon wafer. It is left to cure in a soft bake Oven for 2 hours. In order to increase the surface energy of the PDMS for better adhesion to the negative photo resist SU-8, the cured PDMS surface is exposed to Oxygen Plasma for 33 seconds immediately following which SU-8 2100 is spin coated on the PDMS to a thickness of ~10 microns.

This is left to dry on a hot plate at 65 degrees Celsius for 30 minutes followed by 95 degrees for another 30 minutes. Using a dark field photomask, the SU-8 is exposed to near UV radiation for 3 bursts of 20 seconds each separated by 10 second intervals. The Silicon Wafer is then allowed to bake on a hot plate at 65degrees for 30 minutes followed by 95 degrees for another 30 minutes. After cooling down the wafer is developed in a solution of Poly Mono Acetate (PMA) and is washed with isopropanol.

The SU-8 pattern after this stage is shown in Figure 3.7. This wafer is then coated with a 60 micron layer of Soft PDMS. And SU-8 is again coated and developed on this as described in the process above. Finally a 20 micron layer of PDMS is spin coated to complete the device.

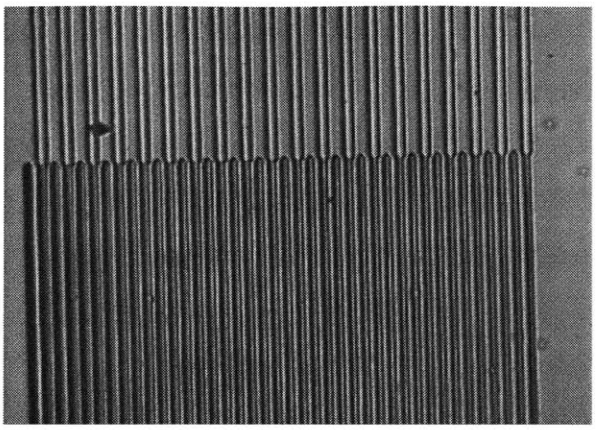

Figure 4.8: Top View of the first layer of SU-8 2100 Pattern on PDMS substrate (after exposure to oxygen plasma) The 5 layer device consists of two such SU-8 layers separated by a layer of Soft PDMS

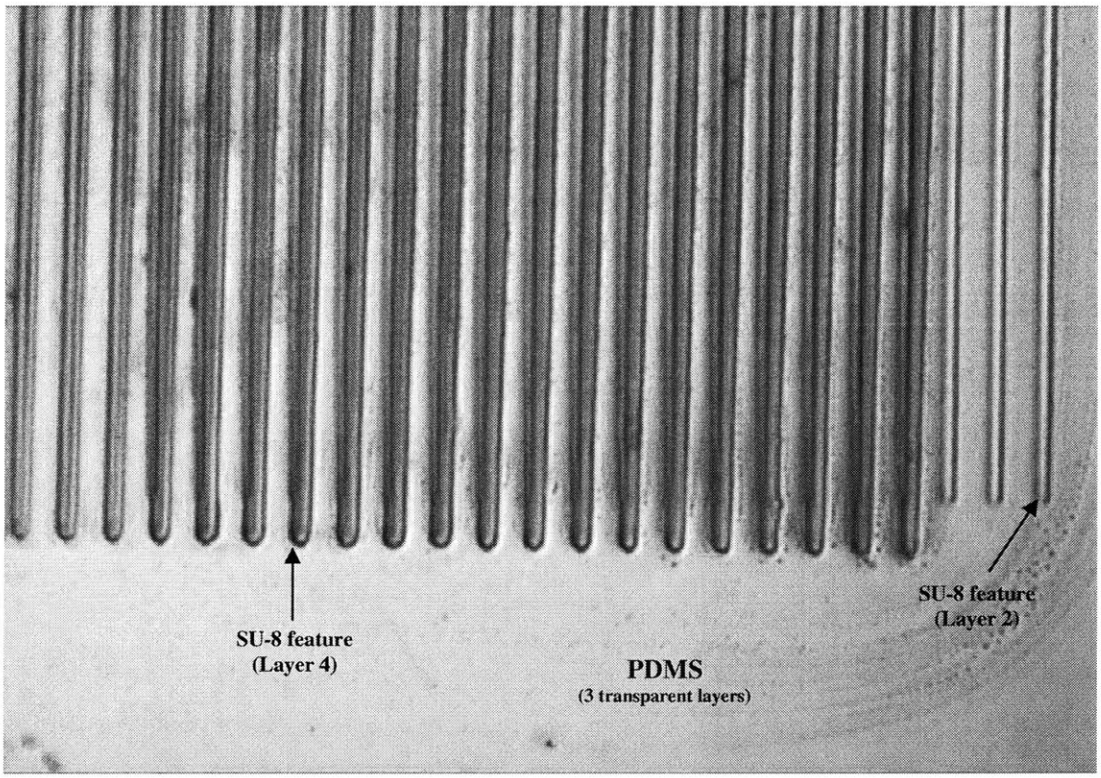

Figure 4.9: Top View of the completed SU-8 pressure sensor. The two SU-8 patterns on the PDMS substrate can be seen. The separation of the parallel bars is 100 microns.

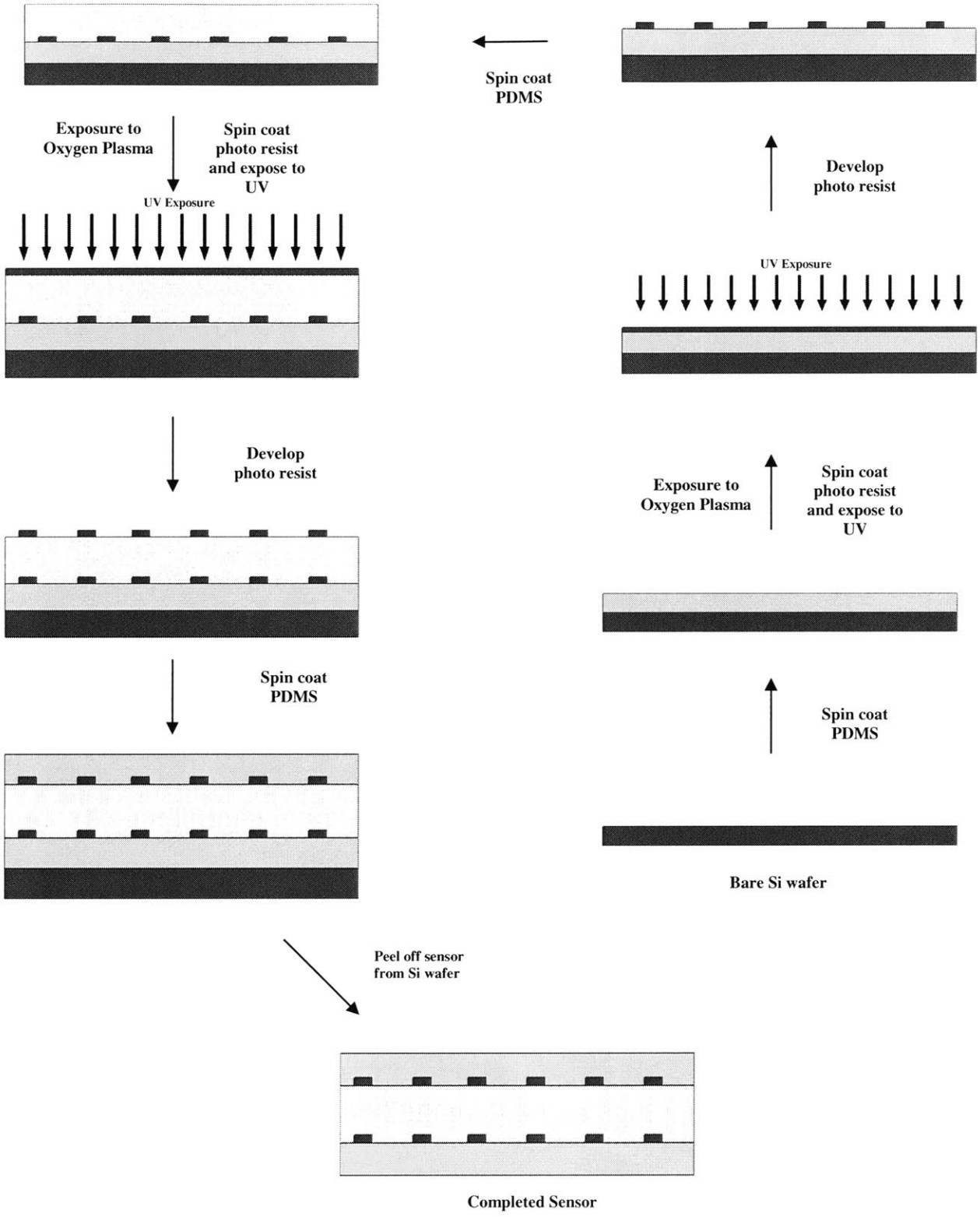

Figure 4.10: Schematic describing the complete process steps in the manufacture of the Pressure Sensor

Chapter 5

Testing and Calibration

This section describes the testing and calibration of the pressure sensor. As has been described in section 2.2, the optical pressure sensor is to be used along with the OCT apparatus to determine pressure at the interface of the sensor and target surface (skin).

5.1 Testing of the fabricated sensor using the OCT

The image of the pressure sensor taken by the OCT apparatus is described in figure 5.1. In this image, the top of the image (bottom layer in contact with the skin) is the bottom of the sensor and in contact with the OCT head.

The pressure sensor consists mainly of transparent PDMS with SU-8 (white translucent) features embedded within the PDMS matrix.

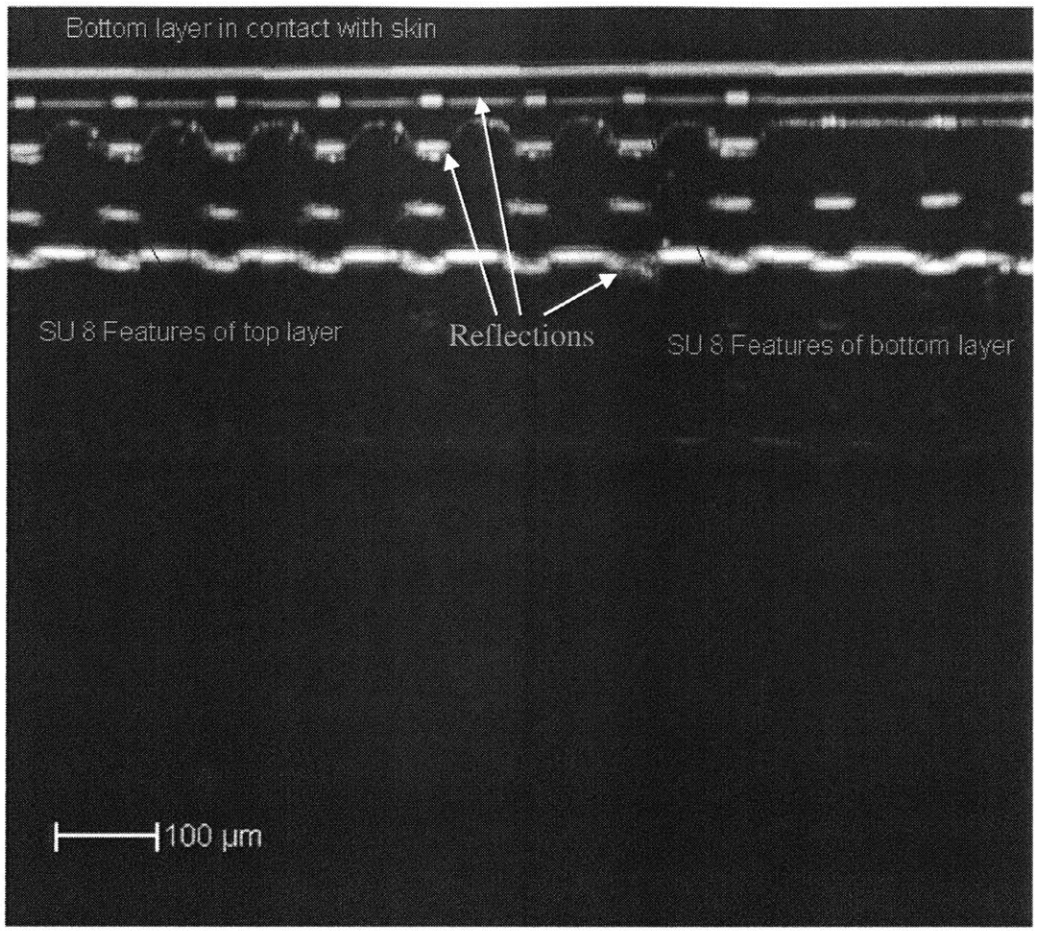

Figure 5.1: OCT image of the fabricated sensor

The OCT image depicted in figure 5.1 shows these SU-8 features. In between these features we can see reflections of these features as well as reflections of the boundaries/edges of the sensor. These arise due to secondary and tertiary reflections of the OCT light source from the features. The OCT functions analogous to sonar with light waves substituting those of sound.

Consider a medium with certain features embedded within the medium, we use a sonar system to non-destructively map a cross section of this medium. The transducer head (which is also a sensor) of the sonar system is placed on the medium and sound waves are transmitted through the medium. When these sound waves encounter an obstacle they reflect back and take this information to the transducer (this backscattered information is used to reconstruct the image of the feature).

However, this back scattered wave is sometimes again reflected back into the medium (either by the transducer head or the boundary of the medium and the transducer head). In the medium this wave encounters the same obstacle and reflects again, transmitting this information to the transducer.

Thus, the transducer interprets this as another feature within the matrix and generates another feature in the image. Analogous to this, the OCT system also generates reflections within the image (indicated in figure 5.1).

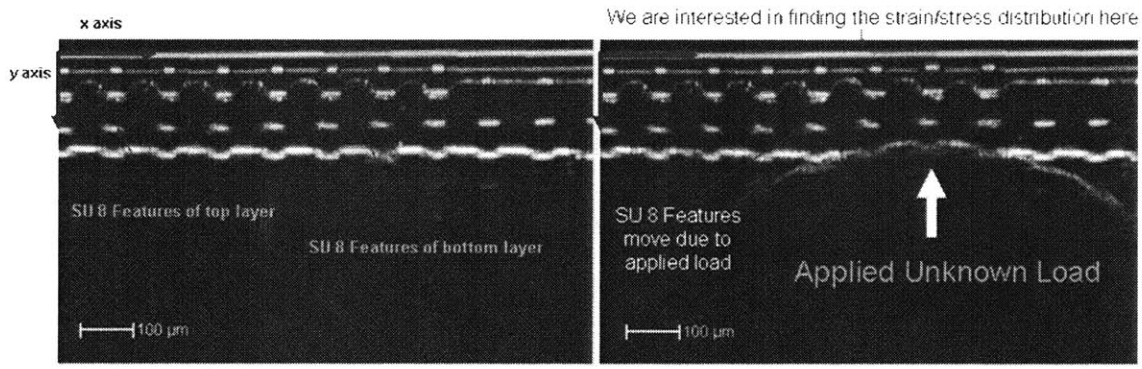

Figure 5.2: OCT images of the a) undeformed sensor and b) the deformed sensor

The procedure by which we will determine the pressure distribution at the interface of sensor and the test surface is through the analysis of two images taken in succession. The first image (as fig. 5.2 (a)) would be of the sensor in an undeformed configuration. This image would give us the reference state.

A MATLAB code is written which calculates the positions of the centroids of each of the features and tabulates it. The program includes the provision of excluding a user defined region which consists of all the reflections within the image, thus excluding these from all calculations.

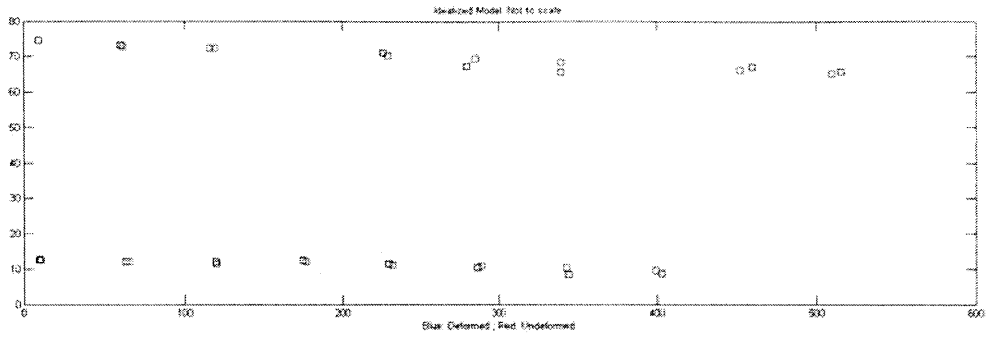

Figure 5.3: MATLAB identification and regeneration of the features. The Blue squares denote the centroids of the deformed features whereas the red squares denote those of the undeformed features. (Note: features with too much noise have been omitted in the calculations)

The unknown load is now incident on the sensor and another image is taken in this deformed configuration. The MATLAB program again determines and tabulates the location of the centroids of the deformed features.

The X and Y deformations of each of the features are then calculated. The continuum mechanics model, developed in chapter 3, is used to determine the stress distribution due to the indentation at the sensor and OCT head interface.

5.1.2 Image Processing

The images captured by the OCT do have a lot of noise (mainly reflections and speckles). In order to examine the images and determine the displacements of the features we need to preprocess the image in an attempt to reduce noise before using the images to calculate the deformations. However, image processing has been kept at a minimum and in order to work around the problem the code excludes some sections from the image which contain noise.

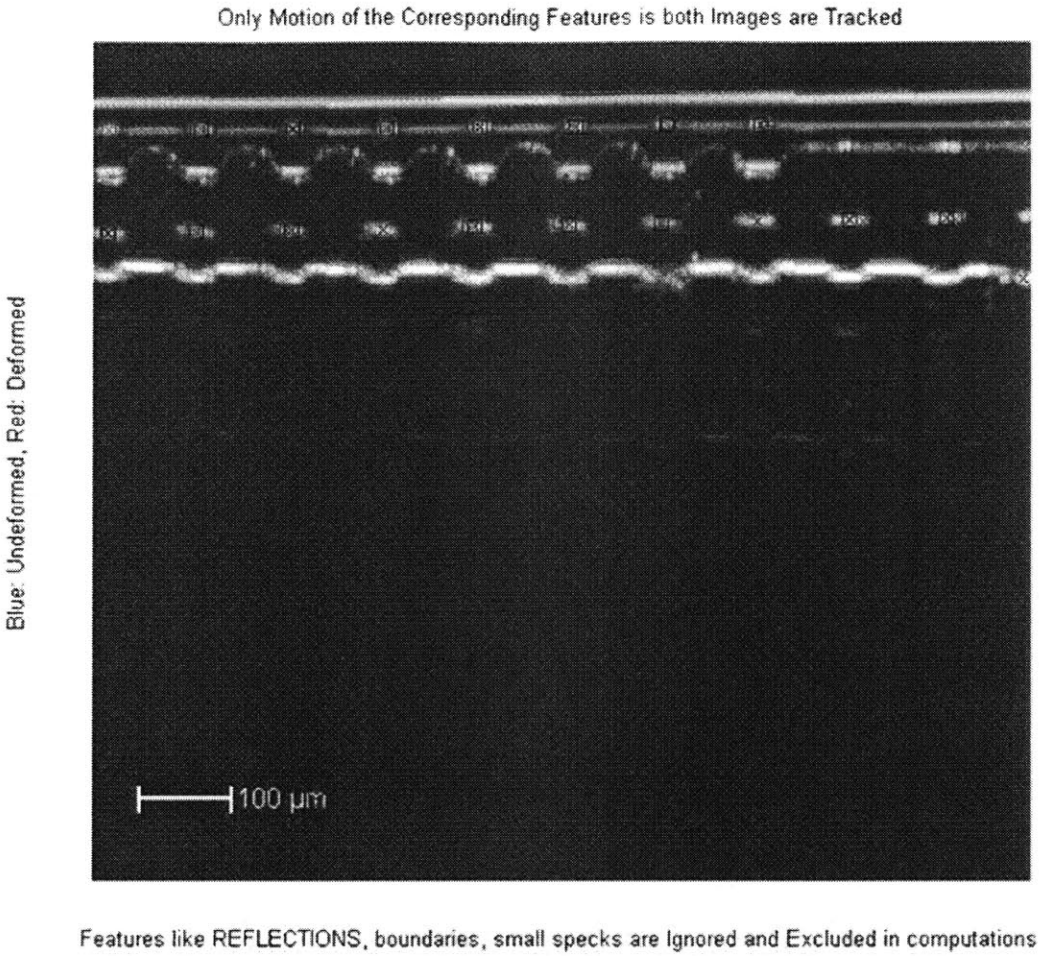

Figure 5.4: Computation of the deformations of each of the features. The blue boxes indicate the centroids of the undeformed features and the red boxes that of the deformed features.

5.2 Calibration tests

In order to calibrate the sensor, we perform experiments to determine the sensitivity and load limits of the sensor.

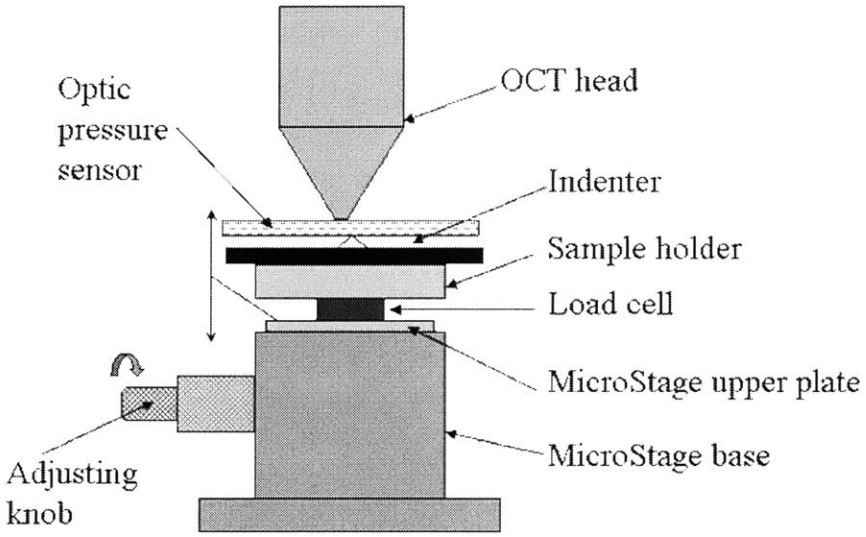

Figure 5.5: Schematic of the Calibration setup

The sensor calibration setup is described in figure 5.5. The calibration test involves indenting the sensor with a micro indenter (fabricated via photolithography on a glass slide coated with a photoresist). The setup consists of a z stage fitted with a load cell, a micro indenter, the optical pressure sensor and the OCT apparatus. The pressure sensor is placed on the OCT head and the indenter, loaded onto the z stage fitted with a load cell, is pressed against the sensor.

We indent the sensor with the micro needle and observe the deformations of the features and determine the strain distributions using our model.

5.3 Results

The first set of tests we performed was to test the maximum displacement of the sensor in response to applied load. We applied sharp indenters of different weights on the sensor

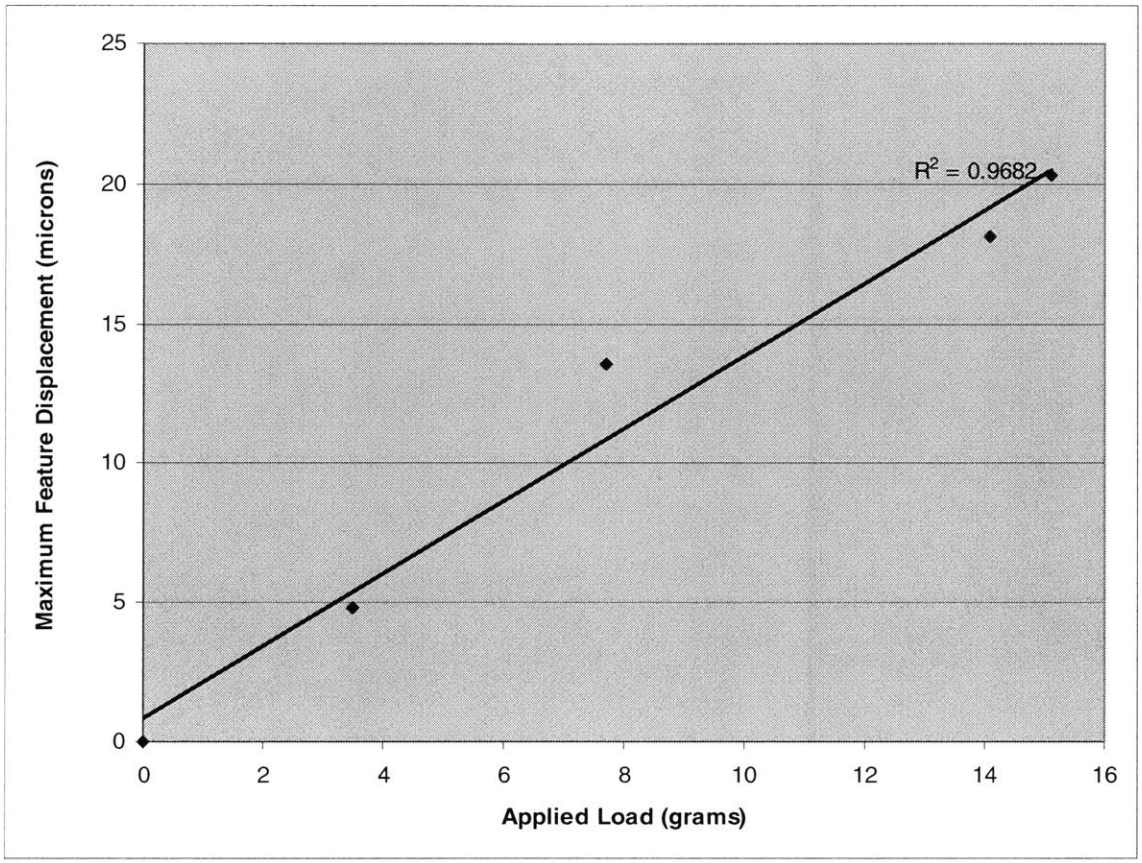

Figure 5.6: Calibration plot between the applied load of the sensor and maximum feature displacement within the sensor.

The relationship is linear with $R^2 = 0.9682$. We find that the load limit of the sensor is 20 grams for a pointed tip load. Beyond this point the features are not clearly visible as the features interfere with the reflections and the MATLAB code cannot pick up the deformations.

This calibration plot shows that the sensor is a linear element.

We now use the model to predict the peak normal stress due to these loads through our model.

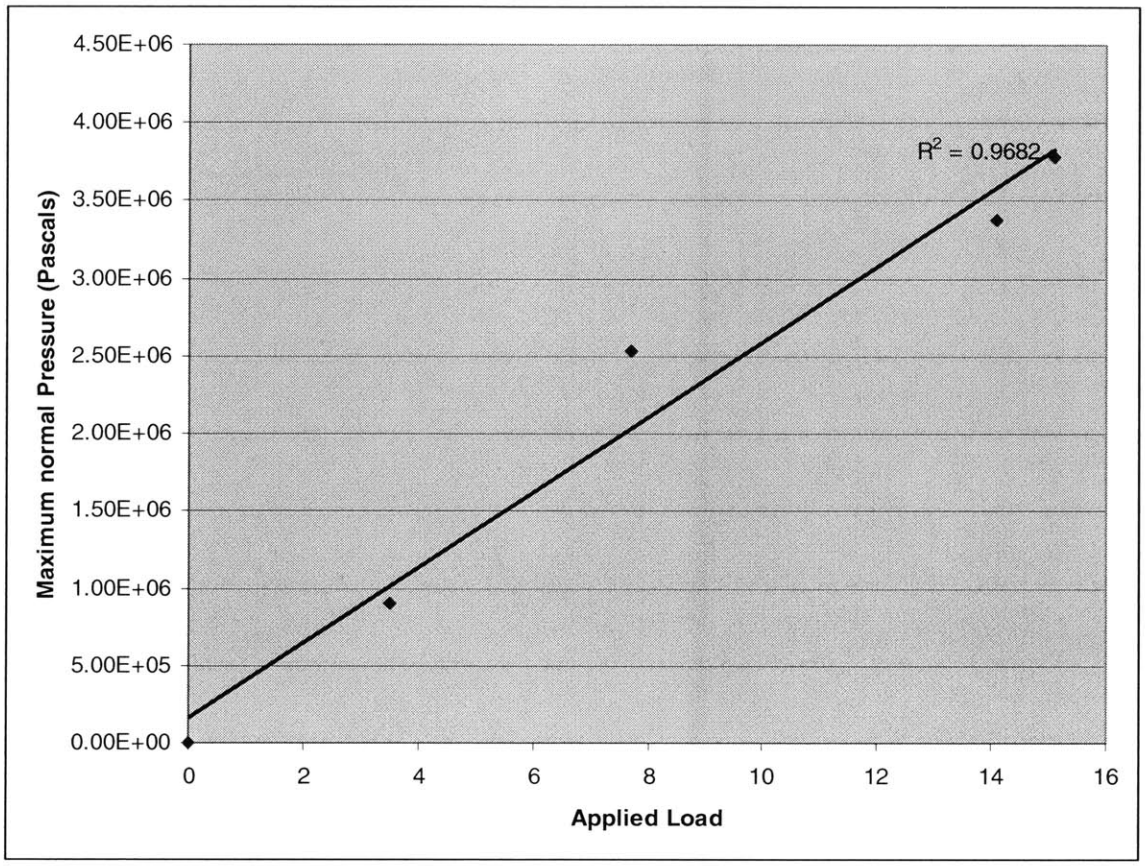

Figure 5.7: Calibration plot between the applied load of the sensor and maximum normal stress.

We now use the sensor element to determine the normal and shear strains and stress distributions due to a pointed indenter (ball point pen tip weighing 3.5 gms)

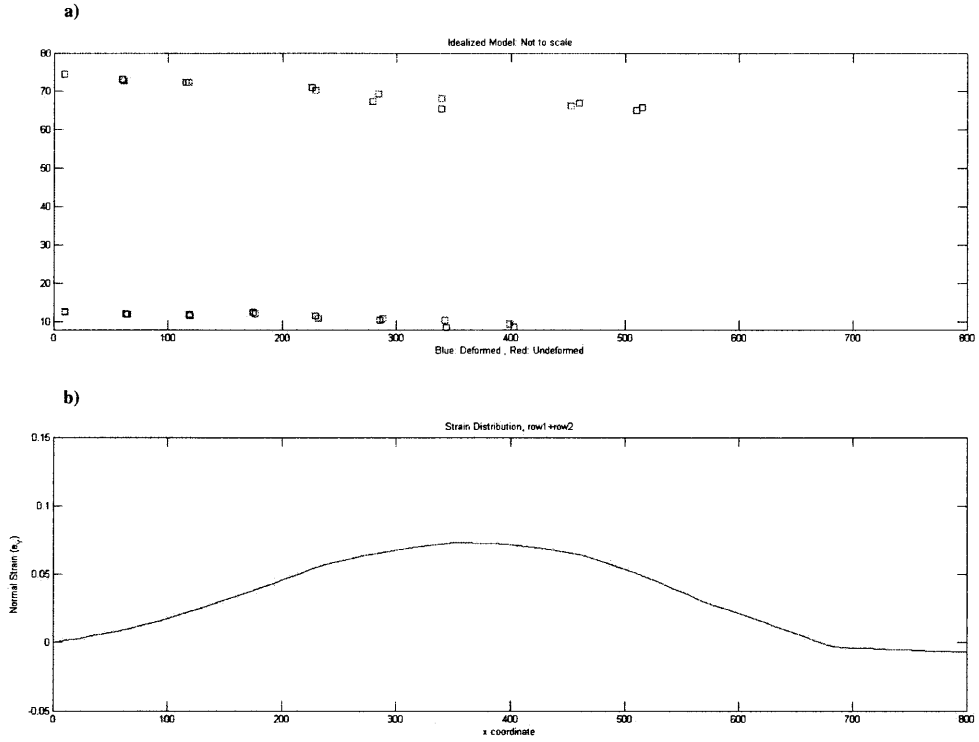

Figure 5.8: Figure (a) depicts the MATLAB reconstruction of the feature displacements due to a load applied by a ball point pen weighing 3.5 grams. Figure (b) depicts the normal strain exerted by the ball point pen.

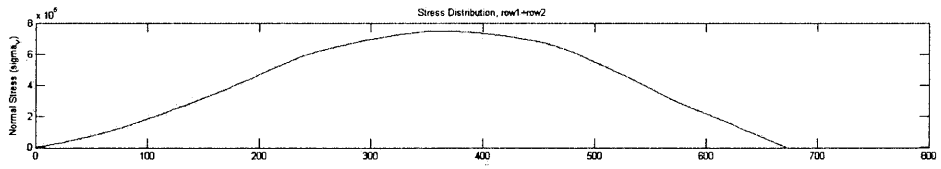

Figure 5.9: Figure depicts normal stress exerted due to a load applied by a ball point pen weighing 3.5 grams.

The plot depicts a peak stress of 0.75 M Pa exerted by the tip of a ball point pen. It exerts a stress field over a distance of 800 microns. It is to be noted that at around 670 microns the sensor leaves contact with the OCT head resulting in zero stress beyond that point.

Chapter 6

Conclusions and Future Work

6.1 Thesis Summary and Contributions

This thesis presents the design of a novel PDMS based flexible pressure micro-sensor with a spatial resolution of **50** microns capable of measuring normal and shear stress exerted by a micro-indenter. The sensor was fabricated bottom up using soft lithography techniques on a silicon wafer. The negative photo resist SU-8 was tested and selected as the material for the developing patterns on PDMS. The five layer device was fabricated on the Silicon wafer and peeled off onto glass slides for testing and calibration.

The device is used in conjunction with an OCT apparatus to determine the deflection of the two layers of patterns. MATLAB routines were developed to identify and track the motion of the features

The OCT images and successive MATLAB code determine the displacement of a finite number of points (SU-8 features) within the PDMS matrix. It was required to determine stress at the sensor-finger interface using this information only.

As the sensor is also to be used with loads of undefined geometry, the load geometry characteristics were not taken into the account when determining the stress. The challenge was to determine the inverse solution using this partial information and boundary conditions where displacement information of a finite number of points within the matrix was known and the stress distribution within the matrix was to be found out.

A continuum mechanics model of the sensor was developed to determine the strain and hence stress distribution at the sensor-finger interface. This was also programmed into MATLAB.

The software is designed to input two images of the sensor (undeformed and deformed) and identify and calculate the displacements of each of the SU-8 features within the matrix. This displacement information is used to determine and plot the normal and shear stress and strain plots at the sensor and finger interface through the continuum mechanics model.

The testing and calibration of the device was done to determine its working range, sensitivity and characteristics. The sensor was indented with indenters of different widths for different depths and the strain distributions at the sensor interface were determined using the model.

6.2 Sensor Characteristics

1. Spatial resolution: 50 microns (distance between the embedded features)
2. Measurable Pressure: Linear behavior observed up to an applied pressure of 3.79 M Pa
3. Effective working area = .01 mm^2 (this refers to the spatial range over which pressure can be measured)
4. Sensitivity: 1 micron (smallest deflection of features that can be picked up by the OCT and image processing)

6.3 Future work

6.3.1 Optimizing the Sensor Design

The sensor is designed to have a spatial resolution of 50 microns. This is dependent on the feature size and spacing between the photoresist bars. Sensor characteristics can be improved by fabricating the sensor with finer features (smaller bars). However this is limited by the OCT resolution and fabrication methods (mentioned below). The OCT image resolution in the X direction (along the plane of the sensor) is 3 microns and that in the Y direction (normal to the plane of the sensor) is 5 microns.

In addition to this making the sensor very thin (below 100 microns) would add complications while peeling the sensor from the Si wafer. Presently the sensor is 150 microns thick and peeling is done with great care using a blade. Sensors with thicknesses below 100 microns would require the development of alternative and reliable techniques for peeling the thin polymer film from the Si wafer without damaging the sensor.

6.3.2 Improvements in the Fabrication Steps

As mentioned above, the smallest feature size that can be fabricated on the sensor is 3 by 5 microns due to the limitations of the OCT apparatus. Such feature sizes would require better control in the manufacturing processes. Currently we fabricate the sensor using soft lithography techniques and develop the features over PDMS using photolithography. One of the challenges faced during the development of the sensor was the adhesion between the polymer and the resist.

Though exposure to oxygen plasma did improve the adhesion at the interface better techniques need to be to improve the adhesion between PDMS and the resist need to be developed. One approach could be through the use of different materials. One such alternative could be substituting the resist with photo pattern able silicone.

6.3.3 Improvements in the development of the continuum mechanics model;

Our continuum mechanics model is developed under many assumptions to simplify its derivation. The model can be used to better describe the sensor taking into account the large feature sizes. In our derivation, we reduce the resist features to a point to simplify computations. The continuum mechanics model could be improved by assuming the features to be of finite shapes having a very large elastic modulus (we assume them to be undeformable under the loading conditions).

6.3.4 Design software for Dynamic loading.

The sensor has been designed to work for static loads only. Successive images of the sensor under static loading (undeformed and deformed images) are taken and they are processed to determine the strain distribution due to an unknown incident load. This method can be extended to accommodate loading at different times. More work could be done on the software to improve the speed of image acquisition from the OCT and its processing to enable dynamic loading as well.

6.4 Application

The pressure sensor was developed to be used along with Optical Coherence Tomography (OCT) apparatus to measure the spatial pressure distribution at the contact interface between external stimuli and (a) the in vitro skin samples as well as (b) in vivo human finger pads together with simultaneous imaging of corresponding skin layer deformations.

We will also use the OCT to image the deformation of the skin layers caused by the external stimuli. Similar experiments will be performed in vivo on the human finger pad to characterize the differences between the mechanical behaviors of in vitro monkey skin sample and in vivo human fingerpad skin.

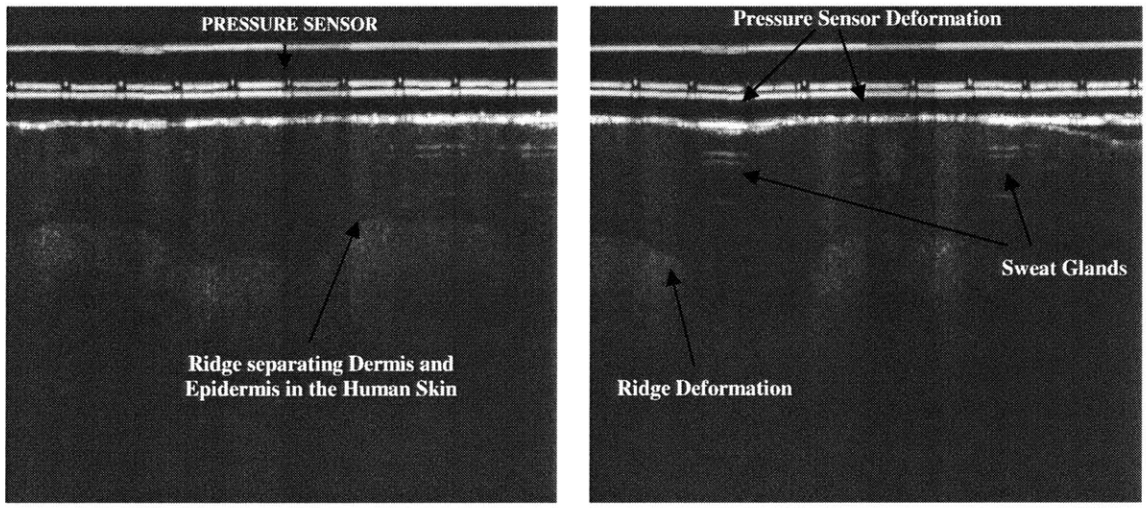

Figure 6.1 : In vivo images of the Human Fingertip (With the Pressure Sensor) taken with the OCT (a) Un-deformed Configuration (b) Deformed Configuration (flat indenter)

During application, the pressure sensor is placed between the OCT head and the finger pad to be imaged. The OCT head along with the stimulus (figure 6.2) also acts as the mechanical stimulus and thus indents the fingerpad. As a result of this deformation the human skin along with the pressure sensor gets deformed. Both these deformations are picked up by the OCT image.

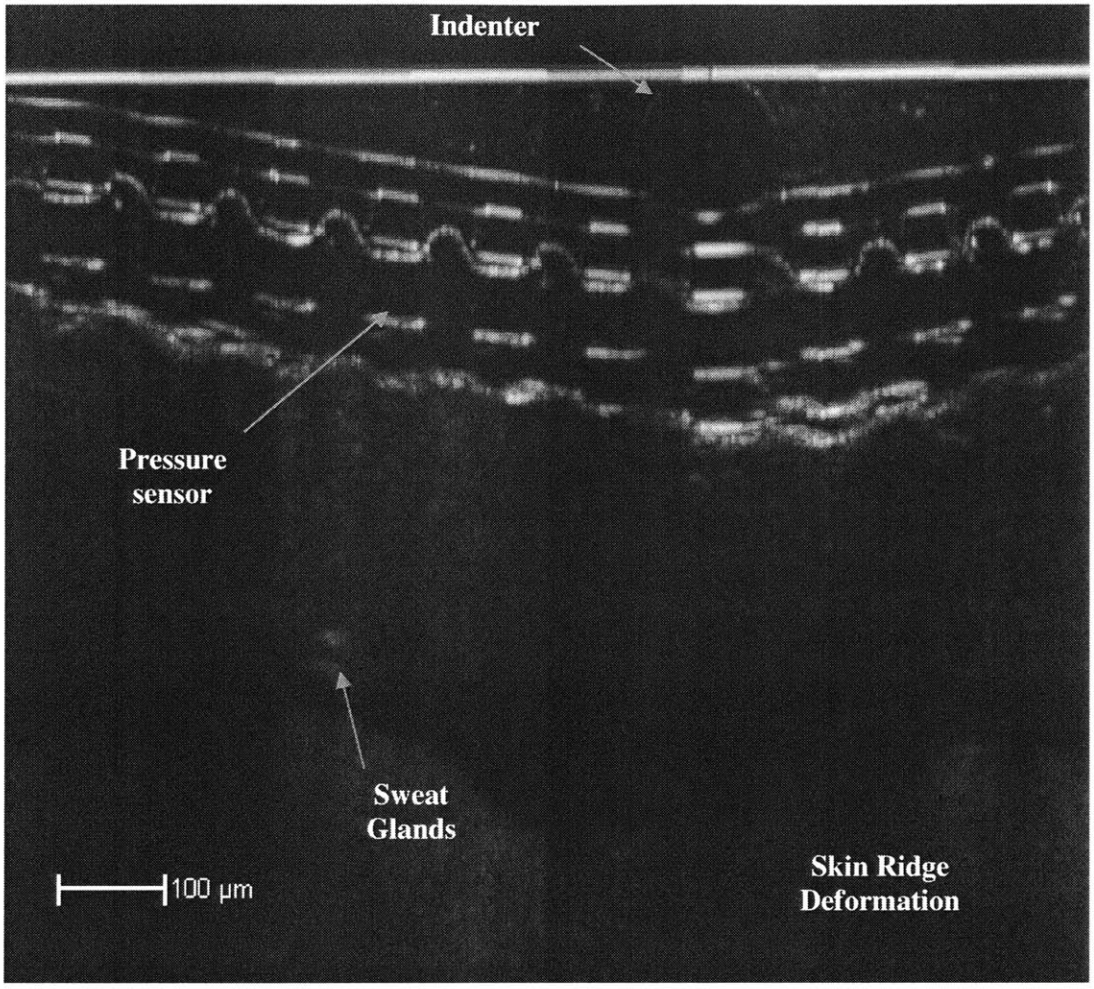

Figure 6.2 : A picture showing the pressure sensor used with an indenter (125µm optical fiber) to see deformations within the skin

The deflection between the two bands of SU-8 is used to estimate the stress in the pressure sensor and hence pressure distribution incident on the skin as the mechanical properties of the all components of PDMS is known.

References

[1] Schmitt J M, Optical Coherence Tomography (OCT): A Review IEEE JOURNAL OF SELECTED TOPICS IN QUANTUM ELECTRONICS, VOL. 5, NO. 4, JULY/AUGUST 1999

[2] Stephan A. Boppart, Brett E. Bouma, Costas Pitris, James F. Southern, Mark E. Brezinski & James G. Fujimoto, "In vivo cellular optical coherence tomography imaging", Nature Medicine 4, 861 - 865 (1998)

[3] Voss, K. J. and M. A. Srinivasan. "Investigation of the Internal Geometry and Mechanics of the Human Fingertip, in vivo, using Magnetic Resonance Imaging" Touch Lab Report 10. RLE TR-622. MIT. Cambridge (1998).

[4] Johnson K. O., "The roles and functions of cutaneous mechanoreceptors", Current Opinion in Neurobiology (2001) 11:455-461

[5] Srinivasan, M. A. and K. Dandekar (1996). "An investigation of the mechanics of tactile sense using two dimensional models of the primate fingertip", Journal of Biomechanical Engineering 118: pp. 48-55.

[6] Dandekar, K., B.I. Raju and M.A. Srinivasan (2003). "3-D Finite-Element Models of Human and Monkey Fingertips to Investigate the Mechanics of Tactile Sense.", Journal of Biomechanical Engineering, Vol. 125, pp. 682-691, ASME Press.

[7] Johnson, Kenneth O.; Yoshioka, Takashi; Vega-Bermudez, Francisco. "Tactile Functions of Mechanoreceptive Afferents Innervating the Hand.", Journal of Clinical Neurophysiology. 17(6): pp.539-558, November 2000.

[8] Srinivasan MA, Whitehouse JM, LaMotte RH, "Tactile Detection of Slip: Surface Microgeometry and Peripheral Neural Codes", JOURNAL OF NEUROPHYSIOLOGY (1990) Vol. 63, No. 6: pp.1323-1332

[9] Macefield VG, Häger-Ross C and Johansson RS, "Control of grip force during restraint of an object held between finger and thumb: responses of cutaneous afferents from the digits", Experimental Brain Research, Volume 108, Number 1, pp 155 - 171

[10] Brisben A.J., Hsiao S.S. and Johnson K. O. "Detection of Vibration Transmitted hrough an Object Grasped in the Hand", The Journal of Neurophysiology Vol. 81 No. 4 April 1999, pp. 1548-1558

[11] Phillips J.R., Johnson K.O., "Tactile Spatial Resolution III. A continuum Mechanics Model of Skin Predicting Mechanoreceptor responses to bars Edges and Gratings", Journal of Neurophysiology December 1981 Vol. 46, No. 6 pp. 1204-1225

[12] Phillips J.R., Johnson K.O., "Tactile Spatial Resolution II. Neural Representation of Bars, Edges ad Gratings in Monkey Primary Afferents", Journal of Neurophysiology December 1981 Vol. 46, No. 6 pp. 1192-1203

[13] Phillips J.R., Johnson K.O., "Tactile Spatial Resolution I. two point discrimination, Gap Detection, Grating Resolution and Letter Recognition", Journal of Neurophysiology December 1981 Vol. 46, No. 6 pp. 1177-1191

[14] Fuller D.R.G. and Gray J.A.B., The relationship between mechanical displacements applied to the pad and the resultant impulse patterns, J. Physiol. London (1966) Vol. 182, pp. 465-483

[15] Goodwin A.W. and Pierce M.E., Population of quickly adapting mechanoreceptive afferents innervating monkey glabrous skin: representation of two vibrating probes. J. Neurophysiol. (1981). Vol. 45, pp. 243-253

[16] Oliver F. J., Practical Instrumentation Transducers (1971)

[17] Peterson K. E., Silicon as a mechanical material, Proc. IEEE (1982) 70 pp. 420-457

[18] Smith C. S., Piezoresistance effect in germanium and silicon, Phys. Rev. (1954) Vol. 94 pp.42-49

[19] Samaun, Wise K. D. and Angell J. B., An IC Piezoresistive pressure sensor for biomedical instrumentation. IEEE Transc. Biomed. Eng. (1973), BME-20 pp. 101-109

[20] Clark S.K., Wise K.D., Pressure sensitivity in anisotropically etched thin-diaphragm pressure sensors, IEEE Trans. Electron Devices (1979), ED-26, pp.1887-1896

[21] J. A. Dziuban, A. Gorecka-Drzazga and U. Lipowicz, Silicon optical pressure sensor, Sensors Actuators A (1992), Vol. 32, pp. 628-631

[22] Hoppe K, Anderson L. U. A. and Bouwstra S, Integrated Mach-Zehnder interferometer pressure transducer.

[23] Melchiorri C, Slip Detection and Control Using Tactile and Force Sensors, IEEE/ASME TRANSACTIONS ON MECHATRONICS, VOL. 5, NO. 3, SEPTEMBER 2000

[24] Kyberd P. J. ,Chappel P. H., Characterization of an optical and acoustic touch and slip sensor for autonomous manipulation, Meas. Sci. Technol. 3 (10) (1992) pp. 969-975.

[25] Noda K., Hoshino K., Matsumoto K. and Shimoyama I., A shear stress sensor for tactile sensing with the piezoresistive cantilever standing in elastic material, Sensors and Actuators A 127 (2006) pp. *295-301*

[26] S. Okazaki, General reviews on photolithography J. Vac. Sci. Technol. B 1991, 9, 2829 ± 2833

[27] Xia Y., Whitesides G. M., Soft Lithography Angewandte Chemie International Edition Volume 37, Issue 5 , pp. 550 – 575

[28] Pawluk DTP, Son JS., Wellman PS, Peine WJ, Howe RD, A Distributed Pressure Sensor for Biomechanical Measurements, submitted to Journal of Biomechanical Engineering, September 1996.

APPENDIX A:

MATLAB Routines for image processing

Acknowledgements: http://wormsense.stanford.edu/ (Goodman lab at Stanford) for their worm tracker software which helped me understand the basics of feature tracking in successive images.

1. Main Routine for tracking and computing feature deformation

```
%_____
%_____OCT FINAL : SIDDARTH_____
%_____

%OCTfinal inputs 2 jpeg images and identifies and tracks the displacement of only the features while
ignoring reflections

%The user is to define the region within which reflections occur, that
%region will be iognored during processing

%_____%_____
_____LOADING IMAGES Into MATLAB_____
%_____

%Loading Images OCT63.jpg and OCT64.jpg
%Orig greyscale J1, I1
clear;
clc;

[X1,map1] = imread('OCT63.jpg');
I=im2double(X1);
I1=rgb2gray(I);

[X2,map2] = imread('OCT64.jpg');
J=im2double(X2);
J1=rgb2gray(J);
imshow(X2);title('Original Undeformed Image');
y = input('Images loaded (Press Enter)> ','s');

%_____
%_____PRELIM PROCESSING_____
%_____


%creating a mask which shows only intensity > .60 to remove noise and
%unwanted reflections
maskj1=(J1>.65);
maski1=(I1>.65);
```

```
%_____
%_____Creates a mask to block reflections_____
%_____

%BW is the user defined mask that encloses the reflections for removal
%Select reflection region
y = input('Using the mouse cursor, Indicate regions in the image containing REFLECTIONS and double
click when done (Press Enter)> ','s');
BW=roipoly(maskj1);
maskj=(maskj1-BW);
maski=(maski1-BW);

%sprintf('Erasing out Selected Region of Interest')
%figure;

%Orig BW
%subplot(2,2,1);
%imshow(J1);title('Original undeformed Image');

%subplot(2,2,3);
%imshow(I1);title('Original Deformed Image');

%Intensity filtered
%subplot(2,2,2);imshow(maskj);

%Edge detection on the filtered: sobel and log and zercross are good
%options.
edmaskj=edge(double(maskj1),'sobel');
%subplot(2,2,2);imshow(edmaskj);title('Sobel Edge Detection');

edmaski=edge(double(maski1),'sobel');
%subplot(2,2,4);imshow(edmaski);title('Sobel Edge Detection');

%y = input('Undeformed Image and Deformed Processed Images(Press Enter)> ','s');
figure; imshow(edmaskj);title('Undeformed Image');
y = input('Displaying Undeformed Image','s');
figure; imshow(edmaski);title('Deformed Image');
y = input('Displaying Deformed Image','s');
final=edmaski+edmaskj;
%figure;imshow(~final);title('Superposed images showing Deformation using Sobel');
y = input('Tracking and Calculating Feature Coordinates (Press Enter)> ','s');

%_____
%_____POST PROCESSING_____
%_____

%Setting area limits to identify the features; features will be identified
%by having area between minarea and maxarea
MinArea=30;
MaxArea=100;

%Labels binary image each region is labelled
```

```
[L,num]=bwlabel(maskj);
%Each regions properties are stored
stats=regionprops(L,{'Area','Centroid','BoundingBox'});

%Identify feature coordinates and get their centroid, bounding boxes

SU8Indices = find([stats.Area] > MinArea & [stats.Area] < MaxArea);
NumSU8 = length(SU8Indices);
SU8Centroids = [stats(SU8Indices).Centroid];
%SU8Coordinates is arranged as X1 Y1 X2 Y2 and so on where X1Y1 are the
%centroids of the
SU8Coordinates = [SU8Centroids(1:2:2*NumSU8)', SU8Centroids(2:2:2*NumSU8)'];
SU8Sizes = [stats(SU8Indices).Area];

%SU8Box is of the form X1 Y1 Lx1 Ly1 and so on Lx=length of side x
SU8Box=[stats(SU8Indices).BoundingBox];


%_____________________________________________________________________
%_____________ Doing the same for the DEFORMED image_____________
%_____________________________________________________________________

%Labels binary image each region is labelled
[Li,numi]=bwlabel(maski);
%Each regions properties are stored
statsi=regionprops(Li,{'Area','Centroid','BoundingBox'});

SU8Indicesi = find([statsi.Area] > MinArea & [statsi.Area] < MaxArea);
NumSU8i = length(SU8Indicesi);
SU8Centroidsi = [statsi(SU8Indicesi).Centroid];

%SU8Centroids is arranged as X1 Y1 X2 Y2 and so on where X1Y1 are the
%centroids of the Su9Coordinates rearranges them into 2 columns
SU8Coordinatesi = [SU8Centroidsi(1:2:2*NumSU8i)', SU8Centroidsi(2:2:2*NumSU8i)'];
SU8Sizesi = [statsi(SU8Indicesi).Area];

%SU8Box is of the form X1 Y1 Lx1 Ly1 and so on Lx=length of side x
SU8Boxi=[statsi(SU8Indicesi).BoundingBox];

%X coordinates

%Xdef=zeros(round(SU8Coordinatesi/2),1);
m=1;

for k=1:length(SU8Coordinatesi)
  if mod(k,2)==1
    Xdef(m)=SU8Coordinatesi(k);
    m=m+1;
  end
end
```

```
%_____________________________________________________________________
%_____Matching points in deformed and undeformed images_____
%_____________________________________________________________________

%C contains the matching indices: indices in SU8Coordinates and
%SU8coordinatesi that represent the same feature

%We set a limit (max_defl) : the max displacement of any feature
max_defl=10;

i=1;j=1;k=1;

while i<length(SU8Coordinates) & j<length(SU8Coordinatesi)

   if abs(SU8Coordinates(i,1)-SU8Coordinatesi(j,1))<max_defl & abs(SU8Coordinates(i,2)-
SU8Coordinatesi(j,2))<max_defl
      C(k,1)=i;C(k,2)=j;
      i=i+1;j=j+1;k=k+1;
      flag=1;
   end

   if flag==0 & SU8Coordinates(i,1)>SU8Coordinatesi(j,1)
      j=j+1;
   end

   if flag==0 & SU8Coordinates(i,1)<SU8Coordinatesi(j,1)
      i=i+1;
   end

   flag=0;

end

%_____________________________________________________________________
%_____Plotting_____
%_____________________________________________________________________

%Plot centroids and bounding boxes of the features and superpose on the original image

%NOTE we dont plot the reflections; we identify the reflections by a
%paramater Refl = round(Y/10) where Y is the Avg Y value of the reflections

Refl=8;Refl1=7;

%As most reflections have avg Y (ordinate) in the 60s and 70s

figure; imshow(J1);
%imshow(~edmaskj);
hold;

for i=1:length(SU8Coordinates)
     plot(SU8Coordinates(i,1),SU8Coordinates(i,2),'bx');
  end
```

```
for j=1:length(SU8Coordinatesi)
   plot(SU8Coordinatesi(j,1),SU8Coordinatesi(j,2),'rx');
end

%xydisp(i,j) 2D array of X Y displacements of closest points

%Circling features that have deformed < ax_displ


for i=1:length(C)
  plot(SU8Coordinates(C(i,1),1),SU8Coordinates(C(i,1),2),'bs');title('Only Motion of the Corresponding
Features is both Images are Tracked');
  xlabel('Features like REFLECTIONS, boundaries, small specks are Ignored and Excluded in
computations');
  ylabel('Blue: Undeformed, Red: Deformed');
end

for j=1:length(C)
  plot(SU8Coordinatesi(C(j,2),1),SU8Coordinatesi(C(j,2),2),'rs');
end

%FeatureCoord is the x,y coordinates of the features that have moves a max
%of max_displ
%Displacement is the del x, del y of each feature

FeatureCoord=[SU8Coordinates(C(:,1),1),SU8Coordinates(C(:,1),2)];
FeatureCoordi=[SU8Coordinatesi(C(:,2),1),SU8Coordinatesi(C(:,2),2)];

Displacement=FeatureCoord-FeatureCoordi

disp('In microns');
sc=100/56;

in_micron=sc*Displacement

%subplot(2,2,1);imshow
```

2. Subroutine for calculating stress/strains using the continuum mechanics model

```
function ex=p(xi,yi,ui,vi,xmax)
% function inputs the feature coordinates (xi,yi), its displacement
% (ui,vi) and the max feature ordinate (xmax) and outputs an array of stress
% due to the motion of the feature over the defined x:0 to 2*x1max
scl=(100/54)*10^-6;
x1=xi;
y1=yi;
u1=ui;
v1=vi;

% Ordinate of the feature furthest from the origin
x1max=xmax;

% Constants
scl=(100/54)*10^-6;
k=pi/(2*x1);
Cy=k*v1/(2*sinh(k*y1)-tanh(k*y1));

% x extends from 0 to 2* max ordinate of feature. and we plot 100 points
% between these 2 limits and we set e_Y to zeros by default

x=linspace(0,floor(2*x1max));
l=length(x);
e_Y=zeros(1,l);

%PDMS Youngs modulus: 360-870 KPa
E=600000;
nu=.49;
nu1=E/((1-2*nu)*(nu+1));

for i=1:l
   if x(i)<floor(2*x1)
e_Y(i)=Cy*cos(k*(x(i)-x1));
   end
end

Sig_Y=nu1*(1-nu)*e_Y;

ex=Sig_Y;

% figure;plot(x,e_Y)

% Sig_Y=nu1*(1-nu)*e_Y;

% figure;
% subplot(2,1,1); plot(x+xmin,Sig_Y); title('Sigma_Y');
% subplot(2,1,2); plot(x+xmin,Sig_X);title('Sigma_X');
```

```
function ex=p1(xi,yi,ui,vi,xmax)
% function inputs the feature coordinates (xi,yi), its displacement
% (ui,vi) and the max feature ordinate (xmax) and outputs an array of
% strains due to the motion of the feature over the defined x:0 to 2*x1max
scl=(100/54)*10^-6;
x1=xi;
y1=yi;
u1=ui;
v1=vi;

% Ordinate of the feature furthest from the origin
x1max=xmax;

% Constants
scl=(100/54)*10^-6;
k=pi/(2*x1);
Cy=k*v1/(2*sinh(k*y1)-tanh(k*y1));

% x extends from 0 to 2* max ordinate of feature. and we plot 100 points
% between these 2 limits and we set e_Y to zeros by default

x=linspace(0,floor(2*x1max));
l=length(x);
e_Y=zeros(1,l);

%PDMS Youngs modulus: 360-870 KPa
E=600000;
nu=.49;
nu1=E/((1-2*nu)*(nu+1));

for i=1:l
   if x(i)<floor(2*x1)
e_Y(i)=Cy*cos(k*(x(i)-x1));
   end
end

ex=e_Y;

% figure;plot(x,e_Y)

% Sig_Y=nu1*(1-nu)*e_Y;

% figure;
% subplot(2,1,1); plot(x+xmin,Sig_Y); title('Sigma_Y');
% subplot(2,1,2); plot(x+xmin,Sig_X);title('Sigma_X');
```

```
% Stress and Strain plotting Function
% inputs the coordinates of the position of each feature and plots it on
% the idealized model

% Plots the deformations of each feature from the original image
octfinal;

scl=100/54;
% Input the dimensions of the sensor from the figure
xmin=1;
xmax=560;
ymin=40;
ymax=130;

% figure;axis([xmin xmax ymin-40 ymax-40]);title('Idealized Model: Exxagurated in Y
direction');xlabel('Blue: Deformed ; Red: Undeformed');
% box on;hold on;

% l1=xmin:.5:xmax;

% axis equal;

%Tabulating Feature Coordinates and Plotting them in the Idealized model
figure;
subplot(2,1,1);hold on; box on;title('Idealized Model: Not to scale');xlabel('Blue: Deformed ; Red:
Undeformed');
%  plot(l1,ymin-40,'k-');
%  plot(l1,ymax-40,'k-');
for i=1:length(FeatureCoord)
  if FeatureCoord(i,2)<ymax
     plot(FeatureCoord(i,1),FeatureCoord(i,2)-40,'rs');
  end
end


for i=1:length(FeatureCoordi)
  if FeatureCoord(i,2)<ymax
     plot(FeatureCoordi(i,1),FeatureCoordi(i,2)-40,'bs');
  end
end

% Sorts features into row1 and row2
Featuresort;

x=linspace(0,floor(2*xmax));

% plotting Straines for row1

er1=zeros(1,length(x));

for i=1:c
   er1=er1+p1(r1(i,1),r1(i,2),r1(i,3),r1(i,4),xmax);
end
```

```
% subplot(4,1,2);
% plot(x,er1);xlabel('x coordiante');ylabel('Normal Strain (e_Y)');title('Strain Distribution, row1');


er2=zeros(1,length(x));

for i=1:c
   er2=er2+p1(r2(i,1),r2(i,2),r2(i,3),r2(i,4),xmax);
end

% subplot(4,1,3);
% plot(x,er2);xlabel('x coordiante');ylabel('Normal Strain (e_Y)');title('Strain Distribution, row2');

subplot(2,1,2);
er=er2+er1;
plot(x,er);xlabel('x coordinate');ylabel('Normal Strain (e_Y)');title('Strain Distribution, row1+row2');
```